

Ice injected into the tropopause by deep convection – Part 2: Over the Maritime Continent

Dion Iris-Amata¹, Dallet Cyrille¹, Ricaud Philippe¹, Carminati Fabien², Dauhut Thibaut³, and Haynes Peter⁴

¹CRNM, Meteo-France - CNRS, Toulouse, 31057, France

²Met Office, Exeter, Devon, EX1 3PB, UK

³Max Planck Institute for Meteorology, Hamburg, Germany

⁴DAMTP, University of Cambridge, Cambridge, CB3 0WA, UK

Correspondence: iris.dion@umr-cnrm.fr

Abstract. The amount of ice injected up to the tropical tropopause layer has a strong radiative impact on climate. In the tropics, the Maritime Continent (MariCont) region presents the largest injection of ice by deep convection into the upper troposphere (UT) and tropopause level (TL) (from results presented in the companion paper Part 1). This study focuses on the MariCont region and aims to assess the processes, the areas and the diurnal amount and duration of ice injected by deep convection over islands and over seas using a $2^\circ \times 2^\circ$ horizontal resolution during the austral convective season of December, January and February. The model presented in the companion paper is used to estimate the amount of ice injected (ΔIWC) up to the TL by combining ice water content (IWC) measured twice a day in local time in tropical UT and TL by the Microwave Limb Sounder (MLS; Version 4.2) from 2004 to 2017, and precipitation (Prec) measurement from the Tropical Rainfall Measurement Mission (TRMM; Version 007) averaged at high temporal resolution (1 hour). The horizontal distribution of ΔIWC estimated from Prec (ΔIWC^{Prec}) is presented at $2^\circ \times 2^\circ$ horizontal resolution over the MariCont. ΔIWC is also evaluated by using the number of lightning events (Flash) from the TRMM-LIS instrument (Lightning Imaging Sensor, from 2004 to 2015 at 1-h and $0.25^\circ \times 0.25^\circ$ resolutions). ΔIWC^{Prec} and ΔIWC estimated from Flash (ΔIWC^{Flash}) are compared to ΔIWC estimated from the ERA5 reanalyses (ΔIWC^{ERA5}) with the vertical resolution degraded to that of MLS observations ($\langle \Delta IWC^{ERA5} \rangle$). Our study shows that, while the diurnal cycles of Prec and Flash are consistent with each other in timing and phase over land but different over offshore and coastal areas of the MariCont, the observational ΔIWC range between ΔIWC^{Prec} and ΔIWC^{Flash} , interpreted as the uncertainty of our model to estimate the ice injected, is smaller over land (they agree to within - 6 to - 22 %) than over ocean (to within 6 to - 71 %) in the UT and TL. The impact of the vertical resolution on the estimation of ΔIWC is higher in the TL (difference between ΔIWC^{ERA5} and $\langle \Delta IWC^{ERA5} \rangle$) of 32 to 139 % than in the UT (difference of 9 to 33 %). Considering estimates of ΔIWC from all the methods, ΔIWC is estimated in the UT between 4.2 and 10.0 mg m^{-3} over land, and between 0.3 and 4.4 mg m^{-3} over sea, and, in the TL, between 0.5 and 3.7 mg m^{-3} over land and between 0.1 and 0.7 mg m^{-3} over sea. Finally, based on IWC from MLS and ERA5, Prec and Flash, this study highlights that 1) ΔIWC over land ($> 4 \text{ mg m}^{-3}$) has been found to be larger than ΔIWC over sea ($< 4 \text{ mg m}^{-3}$), and 2) small islands with high topography present the largest ΔIWC such as the Java Island (7.7 to 9.5 mg m^{-3} in the UT).

25 1 Introduction

In the tropics, water vapour (WV) and ice cirrus clouds near the cold point tropopause (CPT) have a strong radiative effect on climate (Stephens et al., 1991) and an indirect impact on stratospheric ozone (Stenke and Grewe, 2005). WV and water ice crystals are transported up to the tropopause layer by two main processes: a three-dimensional large-scale slow process (3-m month^{-1}), and a small-scale fast convective process (diurnal timescale) (e.g. Fueglistaler et al., 2009; Randel and Jensen, 2013). Many studies have already shown the impact of convective processes on the hydration of the atmospheric layers from the upper troposphere (UT) to the lower stratosphere (LS) (e.g. Liu and Zipser, 2005; Jensen et al., 2007; Dauhut et al., 2018; Dion et al., 2019). However, the amount of total water (WV and ice) transported by deep convection up to the tropical UT and LS is still not well understood. The vertical distribution of total water in those layers is constrained by thermal conditions of the CPT (Randel et al., 2006). During deep convective events, Dion et al. (2019) have shown that air masses transported up to 146 hPa in the UT and up to 100 hPa in the tropopause layer (TL) have ice to total water ratios of more than 50% and 70%, respectively, and that ice in the UT is strongly spatially correlated with the diurnal increases of deep convection, while WV is not. Dion et al. (2019) hence focused on the ice phase of total water to estimate the diurnal amount of ice injected into the UT and the TL over convective tropical areas, showing that it is larger over land than over ocean, with maxima over land of the Maritime Continent (MariCont), the region including Indonesian islands. For these reasons, the present study is focusing on the MariCont region in order to better understand small-scale processes impacting the diurnal injection of ice up to the TL.

A method to estimate the amount of ice injected into the UT and up to the TL over convective areas and during convective seasons has been proposed by Dion et al. (2019). This method provides an estimation of the amplitude of the diurnal cycle of ice in those layers using the twice daily in local times Ice Water Content (IWC) measurements from the Microwave Limb Sounder (MLS) instrument and the full diurnal cycle of precipitation (Prec) measured by the Tropical Rainfall Measurement Mission (TRMM) instrument, at one hour resolution. The method first focuses on the increasing phase of the diurnal cycle of Prec (peak to peak from the diurnal Prec minimum to the diurnal Prec maximum) and shows that the increasing phase of Prec is consistent in time and in amplitude with the increasing phase of the diurnal cycle of deep convection, over tropical convective zones and during convective season. The amount of ice (ΔIWC) injected into the UT and the TL is estimated by relating IWC measured by MLS during the growing phase of the deep convection to the increasing phase of the diurnal cycle of Prec. Dion et al. (2019) conclude that deep convection over the MariCont region is the main process impacting the increasing phase of the diurnal cycle of ice in those layers.

The MariCont region is one of the main convective center in the tropics with the wettest troposphere and the coldest and driest tropopause (Ramage, 1968; Sherwood, 2000; Hatsushika and Yamazaki, 2001). Yang and Slingo (2001) have shown that, over the Indonesian area, the phase of the convective activity diurnal cycle drifts from land to coastlines and to offshore areas. Even though those authors have done a comprehensive study of the diurnal cycle of precipitation and convection over the MariCont, the diurnal cycle of ice injected by deep convection up to the TL over this region is still not well understood.

Millán et al. (2013) have tentatively evaluated the upper tropospheric diurnal cycle of ice from Superconducting Submillimeter-Wave Limb-Emission Sounder (SMILES) measurements over the period 2009-2010 but without differentiating land and sea over the MariCont, which caused their analysis to show little diurnal variation over that region. Dion et al. (2019) have 1) highlighted that the MariCont must be considered as two separate areas: the MariCont land (MariCont_L) and the MariCont ocean (MariCont_O), with two distinct diurnal cycles of the Prec and 2) estimated the amount of ice injected in the UT and the TL. Over these two domains, it has also been shown that convective processes are stronger over MariCont_L than over MariCont_O. Consequently, the amount of ice injected in the UT and the TL is greater over MariCont_L than over MariCont_O.

60 Building upon the results of Dion et al. (2019), the present study aims to improve their methodology by i) studying smaller study zones than in Dion et al. (2019) and by distinguishing island and sea of the MariCont, ii) comparing the sensitivity of our model to different proxies of deep convection and iii) comparing the amount of ice injected in the UT and the TL inferred by our model to that of ERA5 reanalyses. Based on space-borne observations and meteorological reanalyses, ΔIWC is assessed at a horizontal resolution of $2^\circ \times 2^\circ$ over 5 islands (Sumatra, Borneo, Java, Sulawesi and New Guinea) and 5 seas 70 (West Sumatra Sea, Java Sea, China Sea, North Australia Sea, and Bismarck Sea) of the MariCont during convective season (December, January and February, hereafter DJF) from 2004 to 2017. ΔIWC will be first estimated from Prec measured by TRMM-3B42. A sensitivity study of ΔIWC based on the number of flashes (Flash) detected by the TRMM Lightning Imaging Sensor (TRMM-LIS), an alternative proxy for deep convection as shown by Liu and Zipser (2008), is also proposed. Finally, we will use IWC calculated by the ERA5 reanalyses from 2005 to 2016 to estimate ΔIWC in the UT and the TL over each 75 study zone and compare it to ΔIWC estimated from Prec and Flash.

The observational datasets used in our study are presented in Sect. 2. Method is reviewed in Sect. 3. The amount of ice (ΔIWC) injected up to the TL estimated from Prec is evaluated in Sect. 4. Diurnal cycles of Prec and Flash are compared to each other over different areas of the MariCont in Sect. 5. Results of the estimated ΔIWC injected up to the UT and the TL over five islands and five seas of the MariCont are presented and compared with the ERA5 reanalyses in Sect. 6. Results are 80 discussed in Sect. 7, and conclusions are drawn in Sect. 8. This paper contains many abbreviations and acronyms. To facilitate reading, they are compiled in the Acronyms list.

2 Datasets

This section presents the instruments and the reanalyses used for this study.

2.1 MLS Ice Water Content

85 The Microwave Limb Sounder (MLS, data processing algorithm version 4.2) instrument on board NASA's Earth Observing System (EOS) Aura platform (Waters et al., 2006; Livesey et al., 2018) launched in 2004 provides ice water content (IWC^{MLS} , mg m^{-3}) measurements. MLS data processing provides IWC^{MLS} at 6 levels in the UTLS (82, 100, 121, 146, 177 and 215 hPa). Although optimal estimation is used to retrieve almost all other MLS products, a cloud-induced radiance technique is

used to derive the IWC^{MLS} (Wu et al., 2008, 2009). We have chosen to study only two levels: an upper and a lower level
90 of the TTL. Because the level at 82 hPa does not provide enough significant measurements of IWC to have a good signal-to-
noise, we have selected: 1) 100 hPa as the upper level of the TTL (named TL for tropopause level), and 2) 146 hPa as the
lower level of the TTL (named UT for upper troposphere). MLS follows a sun-synchronous near-polar orbit, completing 233
revolution cycles every 16 days, with daily global coverage every 14 orbits. The instrument crosses the equator twice a day
at fixed times, measuring IWC^{MLS} at 01:30 local time (LT) and 13:30 LT. The vertical resolution of IWC^{MLS} is 4 and 5 km
95 at 146 and 100 hPa, respectively. In our study, high horizontal resolution is now possible because we consider 13 years of
MLS data, allowing the IWC^{MLS} measurements to be averaged within bins of horizontal resolution of $2^\circ \times 2^\circ$ ($\sim 230 \text{ km}^2$).
We select IWC^{MLS} during all austral convective seasons DJF between 2004 and 2017. The IWC measurements were filtered
following the recommendations of the MLS team described in Livesey et al. (2018). The resolution of IWC^{MLS} (horizontal
along the path, horizontal perpendicular to the path, vertical) measured at 146 and 100 hPa is $300 \times 7 \times 4 \text{ km}$ and $250 \times 7 \times 5 \text{ km}$,
100 respectively. The precision of the measurement is 0.10 mg m^{-3} at 146 hPa and 0.25 to 0.35 mg m^{-3} at 100 hPa. While the
accuracy is 100% for values less than 10 mg m^{-3} at both levels, it is strongly reduce by averaging on the study period and over
the study zones. The valid range is 0.1 - 50.0 mg m^{-3} at 146 hPa and 0.02 - 50.0 mg m^{-3} at 100 hPa (Wu et al., 2008).

2.2 TRMM-3B42 Precipitation

The Tropical Rainfall Measurement Mission (TRMM) was launched in 1997 and provided measurements of Prec until 2015.
105 TRMM is composed of five instruments, three of them are complementary sensor rainfall suite (PR, TMI, VIRS). TRMM
had an almost circular orbit at 350 km altitude performing a complete revolution in one and a half hour. The 3B42 algo-
rithm product (TRMM-3B42) (version V7) has been created to estimate the precipitation and extend the precipitation product
through 2019. TRMM-3B42 is a multi-satellite precipitation analysis. The analysis merges microwave and infrared space-
borne observations and included TRMM measurements from 1997 to 2015 (Huffman et al., 2007, 2010; Huffman and Bolvin,
110 2018). Work is currently underway with NASA funding to develop more appropriate estimators for random error, and to intro-
duce estimates of bias error (Huffman and Bolvin, 2018). Prec data are provided at a $0.25^\circ \times 0.25^\circ$ ($\sim 29.2 \text{ km}^2$) horizontal
resolution, extending from 50° S to 50° N (<https://pmm.nasa.gov/data-access/downloads/trmm>, last access: April 2019). Prec
from TRMM-3B42 products does not differentiate between stratiform and convective precipitation. In our study, Prec from
TRMM-3B42 is selected over the austral convective seasons (DJF) from 2004 to 2017 and averaged to a horizontal grid of
115 $2^\circ \times 2^\circ$ to be compared to IWC^{MLS} . The TRMM-3B42 data have been averaged over a 1-hour interval from 0 to 24 hours.
TRMM-3B42 data are provided in Universal Time that we converted into local time (LT). Details of the binning methodology
of TRMM-3B42 is provided by Huffman and Bolvin (2018).

2.3 TRMM-LIS number of Flashes

The Lightning Imaging Sensor (LIS) aboard of the TRMM satellite measures several parameters related to lightning. Accord-
120 ing to Christian et al. (2000), LIS used a Real-Time Event Processor (RTEP) that discriminates lightning events from Earth
albedo light. A lightning event corresponds to the detection of a light anomaly on a pixel representing the most fundamental

detection of the sensor. After spatial and temporal processing, the sensor was able to characterize a flash from several detected events. The observation range of the sensor is between 38° N and 38° S. The instrument detects lightning with storm-scale resolution of 3-6 km (3 km at nadir, 6 km at limb) over a large region (550×550 km) of the Earth's surface. The LIS horizontal resolution is provided at 0.25° × 0.25°. A significant amount of software filtering has gone into the production of science data to maximize the detection efficiency and confidence level. Thus, each datum is a lightning signal and not noise. Furthermore, the weak lightning signals that occur during the day are hard to detect because of background illumination. A RTEP removes the background signal to enable the system to detect weak lightning and improves the detection efficiency during the day. LIS is thus able to provide the number of flashes (Flash) measured. The TRMM LIS detection efficiency ranges from 69% near noon to 88% at night. The LIS instrument performed measurements between 1 January 1998 and 8 April 2015. To be as consistent as possible to the MLS and TRMM-3B42 period of study, we are using LIS measurements during DJF from 2004 to 2015. As LIS is on the TRMM platform, with an orbit that precesses, Flash from LIS can be averaged to obtain the full 24-h diurnal cycle of Flash over the study period with a 1-h temporal resolution. In our study, Flash measured by LIS is binned at 0.25° × 0.25° horizontal resolution to be compared to Prec from TRMM-3B42.

135 2.4 ERA5 Ice Water Content

The European Centre for Medium-range Weather Forecasts (ECMWF) Reanalysis 5, known as ERA5, replaces the ERA-Interim reanalyses as the fifth generation of the ECMWF reanalysis providing global climate and weather for the past decades (from 1979) (Hersbach, 2018). ERA5 provides hourly estimates for a large number of atmospheric, ocean and land surface quantities and covers the Earth on a 30 km grid with 137 levels from the surface up to a height of 80 km. Reanalyses such as ERA5 provide a physically constrained, continuous, global, and homogeneous representation of the atmosphere through combining a large number of observations (space-borne, air-borne, and ground-based) with short-range forecasts. Although there is no direct observation of atmospheric ice content in ERA5, the specific cloud ice water content (mass of condensate / mass of moist air) (IWC^{ERA5}) corresponds to the changes in the analysed temperature (and at low levels, humidity) which is mostly driven by the assimilation of temperature-sensitive radiances from satellite instruments (<https://cds.climate.copernicus.eu/cdsapp!/dataset/reanalysis-era5-pressure-levels-monthly-means?tab=form>, last access: July 2019). IWC^{ERA5} used in our analysis is representative of non-precipitating ice. Precipitating ice, classified as snow water, is also provided by ERA5 but not used in this study in order to focus only on the injected and non-precipitating ice in the TTL. Furthermore, results from Duncan and Eriksson (2018) have highlighted that ERA5 is able to capture both seasonal and diurnal variability in cloud ice water but the reanalyses exhibit noisier and higher amplitude diurnal variability than borne out by the satellite estimates. The present study uses the IWC^{ERA5} at 100 and 150 hPa averaged over DJF from 2005 to 2016 with one-hour temporal resolution. IWC^{ERA5} is governed by the model microphysics which allows ice supersaturation with respect to ice (100-150% in relative humidity) but not with respect to liquid water. Although microwave radiances at 183 GHz (sensitive to atmospheric scattering induced by ice particles) (Geer et al., 2017) are assimilated, clouds and precipitation are not used as control variables in the 4D-Var assimilation system and cannot be adjusted independently in the analysis (Geer et al., 2017). The microwave data have sensitivity to the frozen phase hydrometeors but mainly to larger particles, such as those in the cores of deep convection (Geer

et al., 2017), but the sensitivity to cirrus clouds in ERA5 is strongly dependent on microphysical assumptions on the shape and size of the cirrus particles. Indirect feedbacks are also acting on cirrus representation in the model – e.g. changing the intensity of the convection will change the amount of outflow cirrus generated. This is why observations that affect the troposphere by changing for example the stability, the humidity, or the synoptic situation can affect the upper level ice cloud indirectly (Geer et al., 2017). IWC^{ERA5} is compared to the amount of ice injected in the UT and the TL as estimated by the model developed in Dion et al. (2019) and in the present study. IWC^{ERA5} have been degraded along the vertical at 100 and 150 hPa ($\langle \Delta IWC^{ERA5} \rangle$) consistently with the MLS vertical resolution of IWC^{MLS} (5 and 4 km at 100 and 146 hPa, respectively) using a box function (see section 7.2). IWC^{ERA5} and $\langle \Delta IWC^{ERA5} \rangle$ will be both considered in this study. IWC^{ERA5} , initially provided in kg kg^{-1} , has been converted into mg m^{-3} using the temperature provided by ERA5 in order to be compared with IWC^{MLS} .

3 Methodology

This section summarizes the method developed by Dion et al. (2019) to estimate ΔIWC , the amount of ice injected into the UT and the TL. Dion et al. (2019) have presented a model relating Prec (as proxy of deep convection) from TRMM to IWC^{MLS} over tropical convective areas during austral convective season DJF. The IWC^{MLS} value measured by MLS during the growing phase of the convection (at $x = 01:30$ LT or $13:30$ LT) is compared to the Prec value at the same time x in order to define the correlation coefficient (C) between Prec and IWC^{MLS} , as follows:

$$C = \frac{IWC_x^{MLS}}{Prec_x} \quad (1)$$

The diurnal cycle of IWC estimated ($IWC^{est}(t)$) can be calculated by using C applied to the diurnal cycle of Prec ($Prec(t)$), where t is the time, as follows:

$$IWC^{est}(t) = Prec(t) \times C \quad (2)$$

The amount of IWC injected up to the UT or the TL (ΔIWC^{Prec}) is defined by the difference between the maximum of IWC^{est} (IWC_{max}^{est}) and its minimum (IWC_{min}^{est}).

$$\Delta IWC^{Prec} = C \times (Prec_{max} - Prec_{min}) = IWC_{max}^{est} - IWC_{min}^{est} \quad (3)$$

where $Prec_{max}$ and $Prec_{min}$ are the diurnal maximum and minimum of Prec, respectively. Figure 1 illustrates the relationship between the diurnal cycle of Prec and the two MLS measurements at 01:30 and 13:30 LT. The growing phase of the convection is defined as the period of increase in precipitation from $Prec_{min}$ to $Prec_{max}$. The amplitude of the diurnal cycle is defined by the difference between $Prec_{max}$ and $Prec_{min}$. In Fig. 1, because the growing phase of the convection illustrated is happening

during the afternoon, only the MLS measurement at 13:30 LT is used in the calculation of ΔIWC . IWC at 01:30 LT is not used in that case.

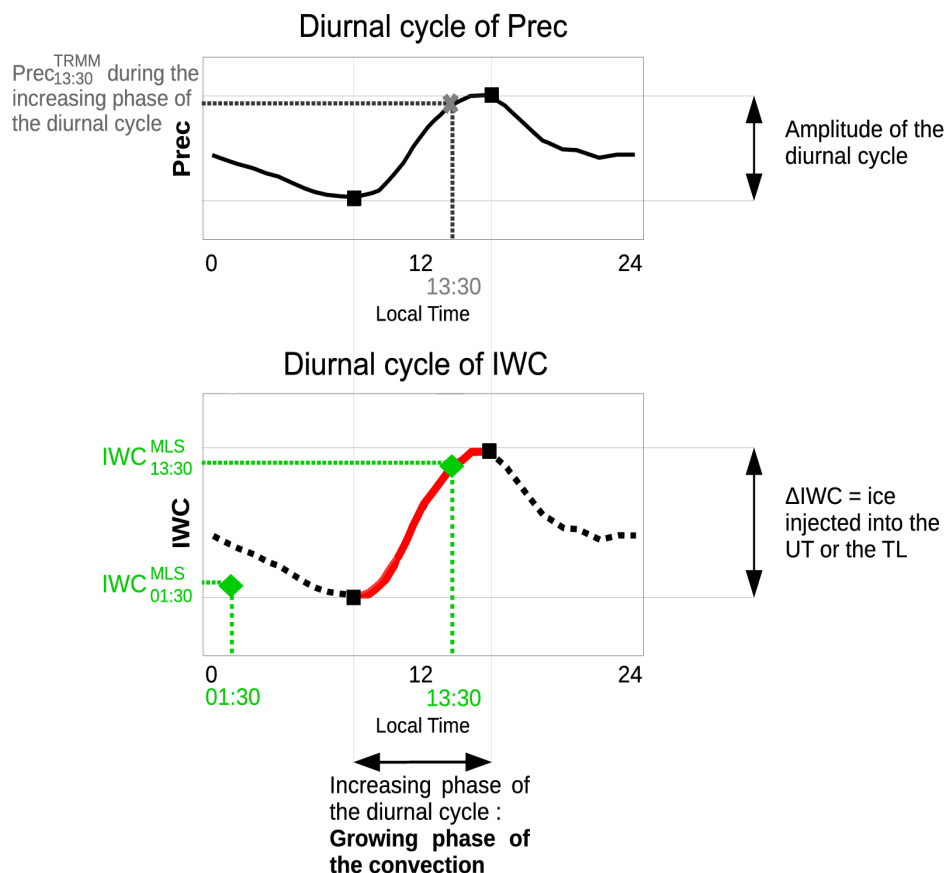


Figure 1. Illustration of the model developed in Dion et al. (2019) to estimate the amount of ice (ΔIWC) injected into the UT or the TL. Diurnal cycle of a proxy of deep convection (Prec) (a), diurnal cycle of ice water content (IWC) estimated from diurnal cycle of the proxy of deep convection (b). In red line, the increasing phase of the diurnal cycle. In black dashed line, the decreasing phase of the diurnal cycle. The green diamonds are the two IWC^{MLS} measurements from MLS. Grey thick cross represents the measurement of Prec during the growing phase of the convection ($Prec_x$), used in the model. Maximum and minimum of the diurnal cycles are represented by black squares. Amplitude of the diurnal cycle is defined by the differences between the maximum and the minimum of the cycle.

4.1 Prec from TRMM-3B42 related to IWC from MLS

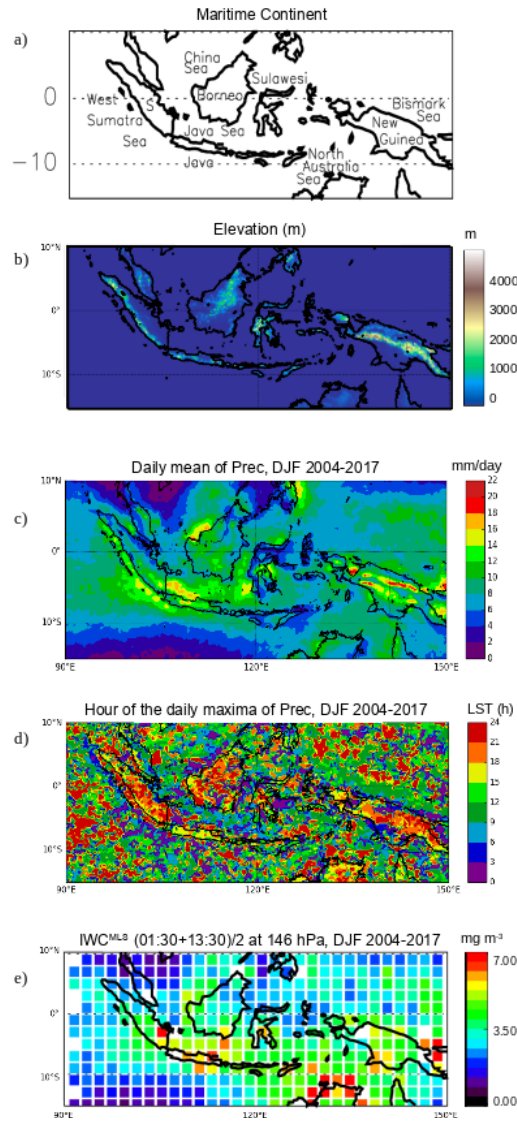


Figure 2. Main islands and seas of the MariCont (S is for Sumatra) (a), elevation from Solar Radiation Data (SoDa) (b); daily mean of Prec obtained from TRMM analysis over the Maritime Continent, averaged over the period of DJF 2004-2017 (c), hour (local solar time (LST)) of the diurnal maxima of Prec over the MariCont (d); daily mean (01:30 LT + 13:30 LT)/2 of IWC^{MLS} at 146 hPa from MLS over the MariCont averaged over the period of DJF 2004-2017 (e). Observations are presented with a horizontal resolution of $0.25^\circ \times 0.25^\circ$ (b, c and d) and $2^\circ \times 2^\circ$ (e).

In order to identify the main areas of injection of ice in the TL over the MariCont, Figure 2 presents different parameters associated to this area: a) the name of the main islands and seas over the MariCont, b) the elevation (<http://www.sodapro.com/web-services/altitude/srtm-in-a-tile>, last access: June 2019), c) the daily mean of Prec at $0.25^\circ \times 0.25^\circ$ horizontal resolution, d) the hour of the diurnal maxima of Prec at $0.25^\circ \times 0.25^\circ$ horizontal resolution, and e) the daily mean ($I\bar{W}C = (IWC_{01:30} + IWC_{13:30}) \times 0.5$) of IWC^{MLS} at 146 hPa at $2^\circ \times 2^\circ$ horizontal resolution. Several points need to be highlighted. Daily means of Prec over land and coastal parts are higher than over oceans (Fig. 2c). Areas where the daily mean of Prec is maximum are usually surrounding the highest elevation over land (e.g. over) and near coastal areas (North West of Borneo in the China Sea and southern Sumatra in the Java Sea) (Fig. 2b and c). The times of the maxima of Prec are over land during the evening (18:00-00:00 LT), over coast during the night-morning (00:00-06:00 TL) and over sea during the morning-noon and even evening depending on the sea considered (09:00-12:00 LT and 15:00-00:00 LT). These differences may be related to the impact of the land/sea breeze over the course of 24 hours. The sea breeze during the day favours the land convection at the end of the day when land surface temperature is higher than oceanic surface temperature. During the night, the coastline sea surface temperature rises above the land surface temperature, and the land breeze systematically favours the development of convection over coasts. These observations are consistent with results presented by Qian (2008), who explained that high precipitation is mainly concentrated over land in the MariCont because of the strong sea-breeze convergence, but also because of the combination with the mountain–valley winds and cumulus merging processes. Amplitudes of the diurnal cycles of Prec over the MariCont will be detailed as a function of island and sea in section 5. The location of the largest concentration of IWC^{MLS} ($3.5 - 5.0 \text{ mg m}^{-3}$, Fig. 2e) is consistent with that of Prec ($\sim 12 - 16 \text{ mm day}^{-1}$) over the West Sumatra Sea, and over the South of Sumatra island. However, over North Australia seas (including the Timor Sea and the Arafura Sea), we observed large differences between Prec low values ($4 - 8 \text{ mm day}^{-1}$) and IWC^{MLS} large concentrations ($4 - 7 \text{ mg m}^{-3}$).

4.2 Convective processes compared to IWC measurements

Although TRMM horizontal resolution is $0.25^\circ \times 0.25^\circ$, we require information at the same resolution as IWC^{MLS} . From the diurnal cycle of Prec in TRMM analysis, the duration of the increasing phase of Prec can be known for each $2^\circ \times 2^\circ$ pixel. The duration of the growing phase of the convection can then be defined from Prec over each pixel. Figures 3a and b present the anomaly (deviation from the mean) of Prec in TRMM-3B42 over the MariCont for the pixels where convection is in the growing phase at 01:30 LT and 13:30 LT, respectively. Anomalies are calculated relative to the average computed over the entire MariCont region. Thus, red colors signify regions that are experiencing the growing phase of convection and whose Prec value is greater than the overall MariCont mean at the respective time (01:30 LT or 13:30 LT), whereas blue colors signify those regions where there is little precipitation compared to the overall MariCont mean during the growing phase of convection. The gray color denotes pixels for which convection is not ongoing. Pixels can be represented in the panels for both local times when: 1) the onset of the convection is before 01:30 LT and the end is after 13:30 LT, or 2) the onset of the convection is before 13:30 LT and the end is after 01:30 LT. Similar anomalies of IWC^{MLS} over the MariCont are shown in Figs. 3c and d, over pixels when the convection is in the growing phase at 01:30 LT and 13:30 LT, respectively. Note that, within each $2^\circ \times 2^\circ$

220 pixel, at least 60 measurements of Prec or IWC^{MLS} at 13:30 LT or 01:30 LT over the period 2004-2017 have been selected for the average.

The Prec anomaly at 01:30 LT and 13:30 LT varies between -0.15 and $+0.15$ mm h^{-1} . The IWC^{MLS} anomaly at 13:30 LT and 01:30 LT varies between -3 and $+3$ mg m^{-3} . At 13:30 LT, the growing phase of the convection is found mainly over land. At 13:30 LT, over land, the strongest Prec and IWC^{MLS} anomalies ($+0.15$ mm h^{-1} and $+2.50$ mg m^{-3} , respectively) are found over the Java island, and northern Australia for IWC^{MLS} . At 01:30 LT, the growing phase of the convection is found mainly over sea (while the pixels of the land are mostly gray), with maxima of Prec and IWC^{MLS} anomalies over coastlines and seas close to the coasts such as the Java Sea and the Bismarck Sea. Three types of areas can be distinguished from Fig. 3: i) area where Prec and IWC^{MLS} anomalies have the same sign (positive or negative either at 01:30 LT or 13:30 LT) (e.g. over Java, Borneo, Sumatra, Java Sea and coast of Borneo or the China Sea); ii) area where Prec anomaly is positive and IWC^{MLS} anomaly is negative (e.g. over West Sumatra Sea); and iii) area where Prec anomaly is negative and IWC^{MLS} anomaly is positive (e.g. over the North Australia Sea at 01:30 LT). Convective processes associated to these three types of areas over islands and seas of the MariCont are discussed in Sect. 6.

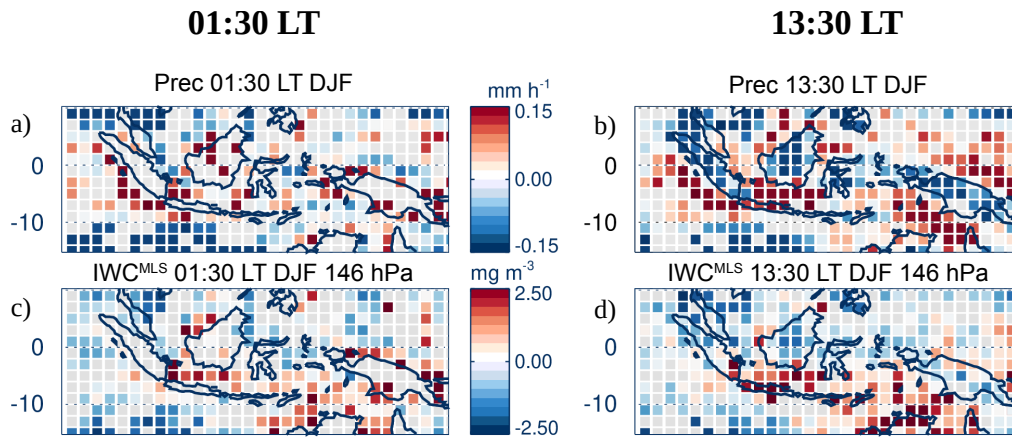


Figure 3. Anomaly (deviation from the mean) of Prec (a-b) and Ice Water Content (IWC^{MLS}) at 146 hPa (c-d), at 01:30 LT (left) and at 13:30 LT (right) over pixels where 01:30 LT and 13:30 LT are during the growing phase of the convection, respectively, averaged over the period of DJF 2004-2017. The gray color denotes pixels for which convection is not ongoing.

4.3 Horizontal distribution of ice injected into the UT and TL estimated from Prec

From the model developed in Dion et al. (2019) based on Prec from TRMM-3B42 and IWC from MLS and synthesized in section 2.4, we can calculate the amount of IWC injected (ΔIWC) at 146 hPa (UT, Figure 4a) and at 100 hPa (TL, Figure 4b) by deep convection over the MariCont. In the UT, the amount of IWC injected over land is on average larger ($> 10 - 20$ mg m^{-3}) than over seas (< 15 mg m^{-3}). Southern Sumatra, Sulawesi, northern New Guinea and northern Australia present the

largest amounts of ΔIWC over land ($15 - 20 \text{ mg m}^{-3}$). Java Sea, China Sea and Bismarck Sea present the largest amounts of ΔIWC over seas ($7 - 15 \text{ mg m}^{-3}$). West Sumatra Sea and North Australia Sea present low values of ΔIWC ($< 2 \text{ mg m}^{-3}$).

240 We can note that the anomalies of Prec and IWC during the growing phase over North Australia Sea at 13:30 LT are positive ($> 0.2 \text{ mm h}^{-1}$, Fig. 3b and $> 2.5 \text{ mg m}^{-3}$, Fig. 3d, respectively). In the TL, the maxima (up to 3.0 mg m^{-3}) and minima (down to $0.2 - 0.3 \text{ mg m}^{-3}$) of ΔIWC are located within the same pixels as in the UT, although 3 to 6 times lower than in the UT. The decrease of ΔIWC with altitude is larger over land (by a factor 6) than over sea (by a factor 3). We can note that the similar pattern between the two layers comes from the diurnal cycle of Prec in the calculation of ΔIWC at 146 and 100 hPa.

245 The differences in the magnitudes of the ΔIWC values at 100 and 146 hPa arise from the different amounts of IWC measured by MLS at those two levels. That is, similar ΔIWC patterns are expected between the two levels because, according to the model developed in Dion et al. (2019), deep convection is the main process transporting ice into the UT and the TL during the growing phase of the convection. Convective processes associated to land and sea are further discussed in Sect. 6.

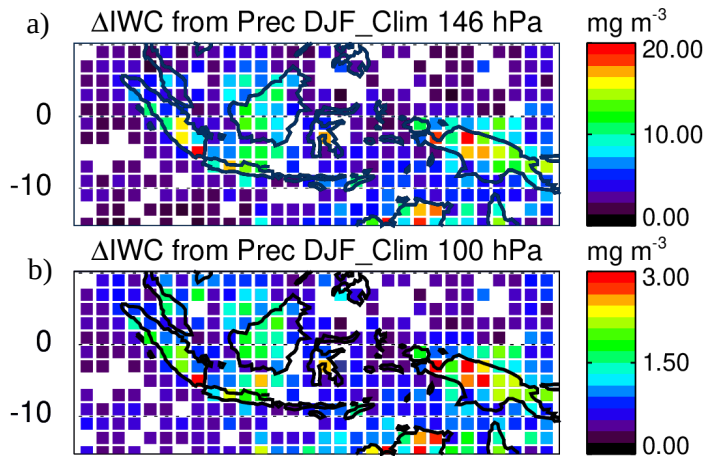


Figure 4. Daily amount of ice injected (ΔIWC) up to the UT (a) and up to the TL (b) estimated from Prec, averaged during DJF 2004-2017.

In order to better understand the impact of deep convection on the strongest ΔIWC injected per pixel up to the TTL, isolated

250 pixels selected in Fig. 4a are presented separately in Figure 5a and f. This Figure shows the diurnal cycles of Prec in four pixels selected for their large ΔIWC in the UT ($\geq 15 \text{ mg m}^{-3}$, Fig. 5b, c, d, e), and the diurnal cycle of Prec in four pixels selected for their low ΔIWC in the UT (but large enough to observe the diurnal cycles of IWC between 2.0 and 5.0 mg m^{-3} , Fig. 5g, h, i, j). Pixels with low values of ΔIWC over land (Fig. 5g, h and i) present small amplitude of diurnal cycles of Prec ($\sim +0.5 \text{ mm h}^{-1}$), with maxima between 15:00 LT and 20:00 LT and minima around 11:00 LT.

255 The pixel with low value of ΔIWC over sea (Fig. 5j) presents an almost null amplitude of the diurnal cycle of Prec, with low values of Prec all day long ($\sim 0.25 \text{ mm h}^{-1}$). Pixels with large values of ΔIWC over land (Fig. 5b, c, d, e) present longer duration of the increasing phase of the diurnal cycle (from $\sim 09:00$ LT to $20:00 - 00:00$ LT) than the increasing phase of Prec

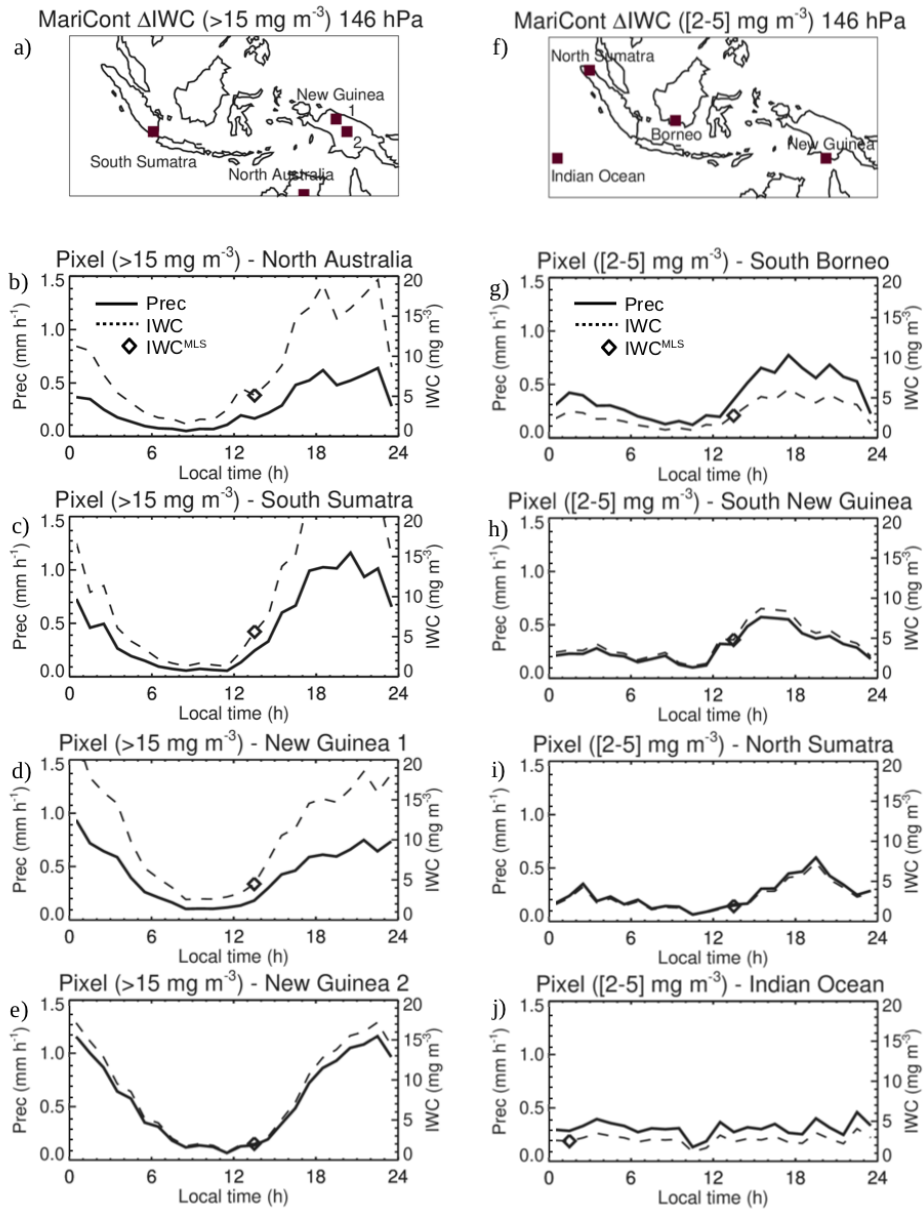


Figure 5. a) and f) Location of $2^\circ \times 2^\circ$ pixels where ΔIWC have been found higher than 15 mg m^{-3} (in Fig. 4) and where ΔIWC have been found between 2 and 5 mg m^{-3} (in Fig. 4), respectively. Diurnal cycle of Prec (solid line): (b, c, d, e) over 4 pixels where ΔIWC have been found higher than 15 mg m^{-3} (in Fig. 4), (g, h, i, j) over 4 pixels where ΔIWC have been found between 2 and 5 mg m^{-3} (in Fig. 4), during DJF 2004-2017. The diamond represents IWC^{MLS} during the increasing phase of the convection. The dashed line is the diurnal cycle of IWC estimated from the diurnal cycle of Prec and from IWC^{MLS} .

diurnal cycle over pixels with low values of ΔIWC (from 10:00 LT to 15:00 – 19:00 LT). More precisely, pixels labeled 1 and 2 over New Guinea (Fig. 5d and e) and the pixel over southern Sumatra (Fig. 5c) show amplitude of diurnal cycle of Prec reaching 1.0 mm h^{-1} , while the pixel over North Australia (Fig. 5b) presents lower amplitude of diurnal cycle of Prec (0.5 mm h^{-1}).

IWC^{MLS} during the growing phase of deep convection and the diurnal cycle of IWC estimated from Prec are also shown on Fig. 5. For pixels with large values of ΔIWC , IWC^{MLS} is between 4.5 and 5.7 mg m^{-3} over North Australia, South Sumatra and New Guinea 1. For pixels with low values of ΔIWC , IWC^{MLS} is found between 1.9 and 4.7 mg m^{-3} . To summarize, large values of ΔIWC are observed over land in combination to i) longer growing phase of deep convection (> 9 hours) and/or ii) large diurnal amplitude of Prec ($> 0.5 \text{ mm h}^{-1}$). However, as IWC^{MLS} ranges overlap for the high and low ΔIWC , no definitive conclusion about the relationship between IWC^{MLS} and ΔIWC can be drawn.

In the next section, we estimate ΔIWC using another proxy of deep convection, namely Flash measurements from LIS.

5 Relationship between diurnal cycle of Prec and Flash over MariCont land and sea

Lightning is created in cumulonimbus clouds when the electric potential energy difference is large between the base and the top of the cloud. Lightning can appear at the advanced stage of the growing phase of the convection and during the mature phase of the convection. For these reasons, in this section, we use Flash measured from LIS during DJF 2004-2015 as another proxy of deep convection in order to estimate ΔIWC (ΔIWC^{Flash}) and check the consistency with ΔIWC obtained with Prec (ΔIWC^{Prec}).

5.1 Flash distribution over the MariCont

Figure 6a presents the daily mean of Flash in DJF 2004-2015 at $0.25^\circ \times 0.25^\circ$ horizontal resolution. Over land, Flash can reach a maximum of 10^{-1} flashes day^{-1} per pixel while, over seas, Flash are less frequent ($\sim 10^{-3}$ flashes day^{-1} per pixel). When compared to the distribution of Prec (Fig. 2c), maxima of Flash are found over similar areas as maxima of Prec (Java, East of Sulawesi coast, Sumatra and northern Australia). Over Borneo and New Guinea, coastlines present more Flash ($\sim 10^{-2}$ flashes day^{-1}) than inland ($\sim 10^{-3}$ flashes day^{-1}). Differences between Flash and Prec distributions are found over North Australia Sea, with relatively large number of Flash ($> 10^{-2}$ flashes day^{-1}) compared to low Prec ($4 - 10 \text{ mm day}^{-1}$) (Fig. 2c), and over several inland areas of New Guinea where the number of Flash is relatively low ($\sim 10^{-2} - 10^{-3}$ flashes day^{-1}) while Prec is high ($\sim 14 - 20 \text{ mm day}^{-1}$). Figure 6b shows the hour of the Flash maxima. Over land, the maximum of Flash is between 15:00 LT and 19:00 LT, slightly earlier than the maximum of Prec (Fig. 2d) observed between 16:00 LT and 24:00 LT. Coastal areas present similar hours of maximum of Prec and Flash, i.e between 00:00 LT and 04:00 LT although, over the West Sumatra Coast, diurnal maxima of both Prec and Flash happen 1–4 hours earlier (from 23:00-24:00 LT) than those of other coasts.

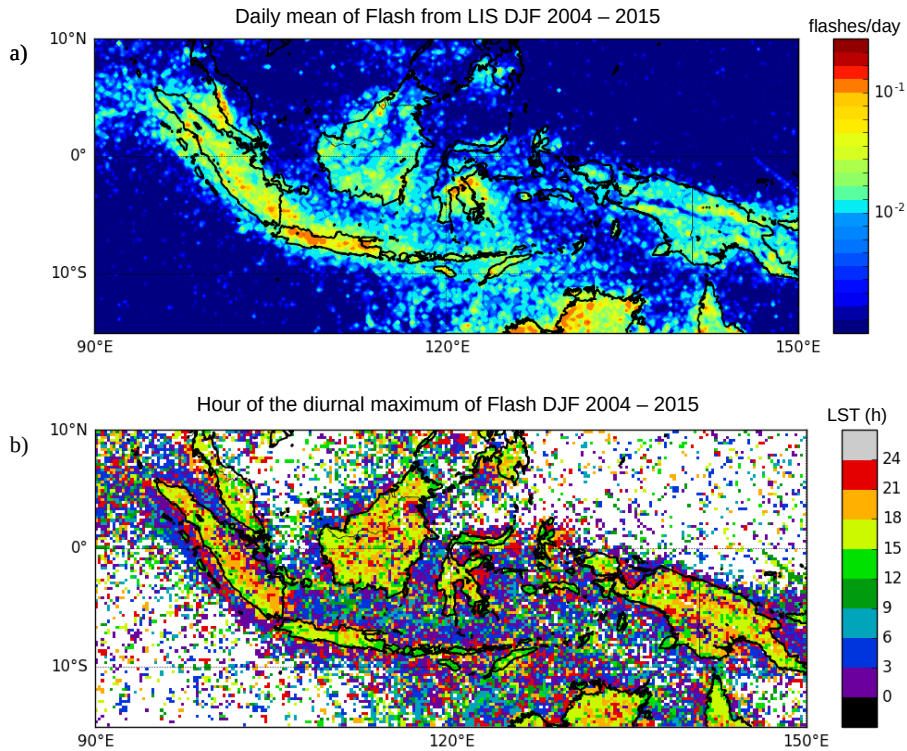


Figure 6. Daily mean of Flash measured by LIS averaged over the period DJF 2004-2015 (a); Hour (local solar time (LST)) of the diurnal maximum of Flash (b).

5.2 Prec and Flash diurnal cycles over the MariCont

This section compares the diurnal cycle of Flash with the diurnal cycle of Prec in order to assess the potential for Flash to be used as a proxy of deep convection over land and sea of the MariCont. Diurnal cycles of Prec and Flash over the MariCont land, coastline and offshore (MariCont_L, MariCont_C, MariCont_O, respectively) are shown in Figs. 7a–c, respectively. Within each $0.25^\circ \times 0.25^\circ$ bin, land/coast/ocean filters were applied from the Solar Radiation Data (SoDa, <http://www.soda-pro.com/web-services/altitude/srtm-in-a-tile>). MariCont_C is the average of all coastlines defined as 5 pixels extending into the sea from the land limit. This choice of 5 pixels was made after consideration of some sensitivity tests in order to have the best compromise between a high signal-to-noise ratio and a good representation of the coastal region. The MariCont_O is the average of all offshore pixels defined as sea pixels excluding 10 pixels (2000 km) over the sea from the land, thus coastline pixels are excluded as well as all the coastal influences. MariCont_L is the area of all land pixels. At the border between the land and the coast areas, a given $0.25^\circ \times 0.25^\circ$ pixel can contain information from both land and coastlines. In that case, we can easily discriminate between land and coastlines by applying the land/coastlines filters. Consequently, this particular pixel will be flagged both as land and coastlines.

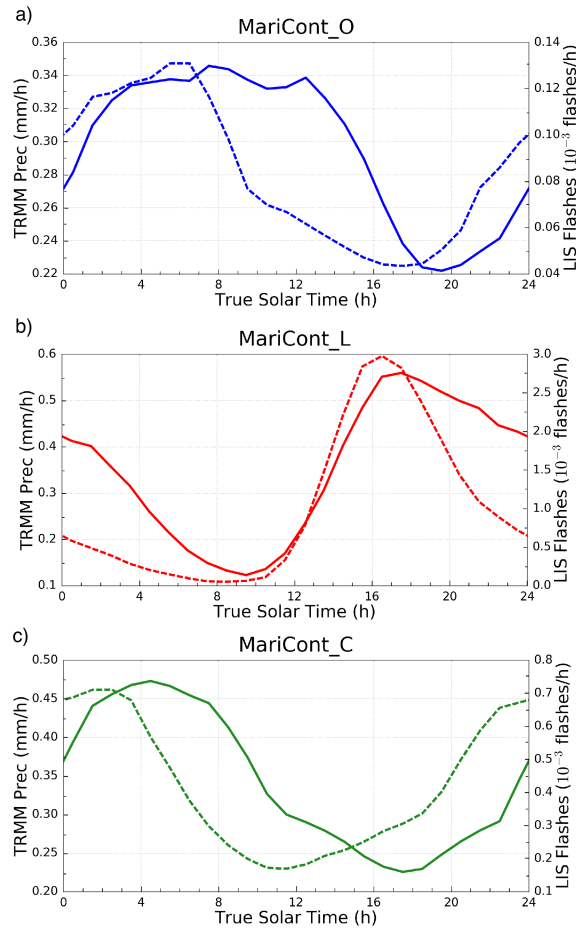


Figure 7. Diurnal cycle of Prec (solid line) and diurnal cycle of Flash (dashed line) over MariCont_L (a), MariCont_C (b) and MariCont_O (c).

300 Over land, during the growing phase of the convection, Prec and Flash start to increase at the same time (10:00 LT – 12:00 LT) but Flash reaches a maximum earlier (15:00 LT – 16:00 LT) than Prec (17:00 LT – 18:00 LT). This is consistent with the finding of Liu and Zipser (2008) over the whole tropics. Different maximum times could come from the fact that, while the deep convective activity intensity starts to decrease with the number of flashes, Prec is still high during the dissipating stage of the convection and takes longer to decrease than Flash. Consequently, combining our results with the ones presented in Dion et al. (2019), Flash and Prec can be considered as good proxies of deep convection during the growing phase of the convection
 305 over the MariCont_L.

Over coastlines (Fig. 7b), the Prec diurnal cycle is delayed by about +2 to 7 h with respect to the Flash diurnal cycle. Prec minimum is around 18:00 LT while Flash minimum is around 11:30 LT. Maxima of Prec and Flash are found around

04:00 LT and 02:00 LT, respectively. This means that the increasing phase of Flash is 2-3 h longer than that of Prec. These
310 results are consistent with the work of Mori et al. (2004) showing a diurnal maximum of precipitation in the early morning
between 02:00 LT and 03:00 LT and a diurnal minimum of precipitation between 11:00 LT and 21:00 LT, over coastal zones
of Sumatra. According to Petersen and Rutledge (2001) and Mori et al. (2004), coastal zones are areas where precipitation
results more from convective activity than from stratiform activity and the amplitude of diurnal maximum of Prec decreases
with the distance from the coastline.

315 Over offshore areas (Fig. 7c), minima of diurnal cycle of Prec and diurnal cycle of Flash are in the late afternoon, between
16:00 LT and 17:00 LT (Flash) and 17:00 LT and 18:00 LT (Prec), whilst maxima of diurnal cycle of Prec and Flash are reached
in the early morning, between 06:00 LT and 07:00 LT (Flash) and around 08:00 LT – 09:00 LT (Prec). Results over offshore
areas are consistent with diurnal cycle of Flash and Prec calculated by Liu and Zipser (2008) over the whole tropical ocean,
showing the increasing phase of the diurnal cycle of Flash starting 1–2 hours before the increasing phase of the diurnal cycle
320 of Prec.

The time of transition from maximum to minimum of Prec is always longer than that of Flash. The period after the maximum
of Prec is likely more representative of stratiform rainfall than deep convective rainfall. Consistent with that picture, model
results from Love et al. (2011) have shown the suppression of deep convection over the offshore area west of Sumatra from
the early afternoon due to a downwelling wavefront characterized by deep warm anomalies around noon. According to the
325 authors, later in the afternoon, gravity waves are forced by the stratiform heating profile and propagate slowly offshore. They
also highlighted that the diurnal cycle of the offshore convection responds strongly to the gravity wave forcing at the horizontal
scale of 4 km. To summarize, diurnal cycles of Prec and Flash show that:

- i) over land, Flash increases proportionally with Prec during the growing phase of the convection,
- ii) over coastlines, Flash increasing phase is more than 6–7 hours ahead of Prec increasing phase,
- 330 iii) over offshore areas, Flash increasing phase is about 1–2 hours ahead of Prec increasing phase.

In section 7, we investigate whether this time difference impacts the estimation of ΔIWC over land, coasts, and offshore
areas.

5.3 Prec and Flash diurnal cycles and small-scale processes

In this subsection, we study the diurnal cycle of Prec and Flash at $0.25^\circ \times 0.25^\circ$ resolution over areas of deep convective
335 activity over the MariCont. In line with the distribution of large value of Prec (Fig. 2), IWC^{MLS} (Fig. 3) and ΔIWC (Fig. 4),
we have selected five islands and five seas over the MariCont. Diurnal cycles of Prec and Flash are presented over land for a)
Java, b) Borneo, c) New Guinea, d) Sulawesi and e) Sumatra as shown in Figure 8 and over sea for the a) Java Sea, b) North
Australia Sea (NAusSea), c) Bismarck Sea, d) West Sumatra Sea (WSumSea) and e) China Sea as shown in Figure 9. Diurnal
cycles of IWC from ERA5 (IWC^{ERA5}) are also presented in Figs. 8 and 9 and will be discussed in Section 6.

340 Over land, the amplitude of the diurnal cycle of Prec is the largest over Java (Fig. 8a), consistent with Qian (2008), with a
maximum reaching 1 mm h^{-1} , while, over the other areas, maxima are between 0.4 and 0.6 mm h^{-1} . Furthermore, over Java,
the duration of the increasing phase in the diurnal cycle of Prec is 6 h, consistent with that of Flash, whereas elsewhere the

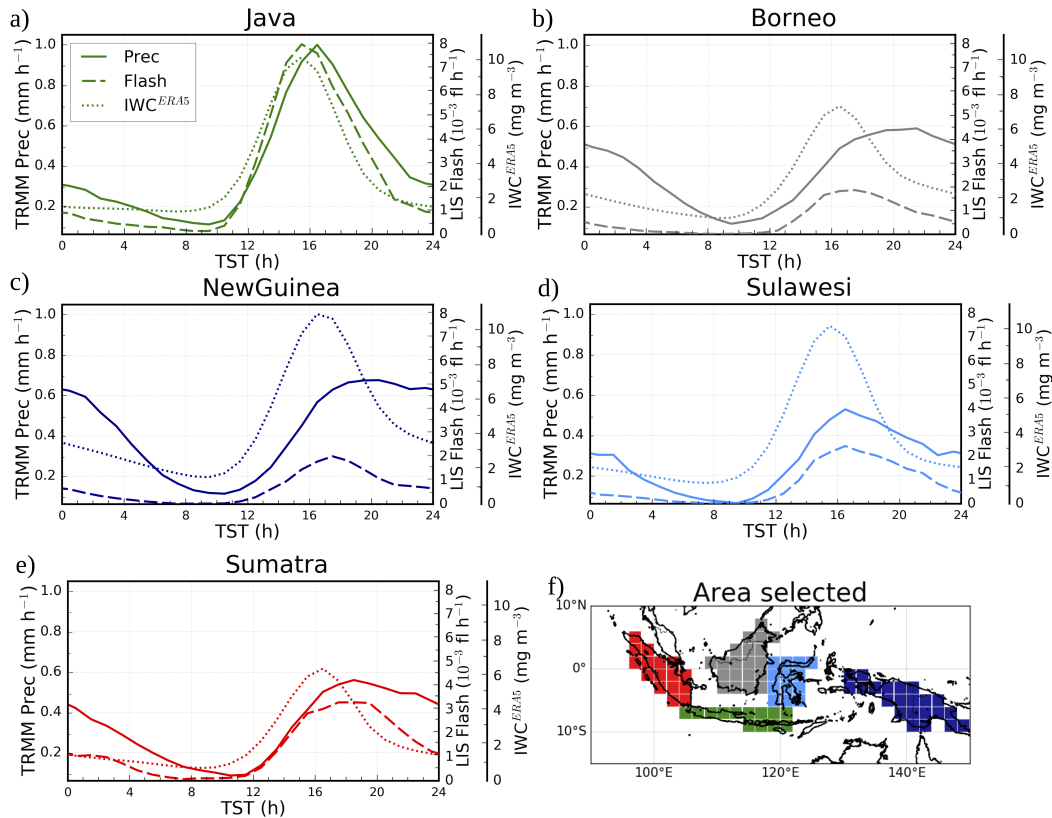


Figure 8. Diurnal cycles of Prec (solid line), Flash (dashed line) and IWC^{ERA5} from ERA5 at 150 hPa (dotted line) over MariCont islands: Java (a), Borneo (b), New Guinea (c), Sulawesi (d) and Sumatra (e) and map of the study zones over land (f).

duration of the increasing phase is longer in Prec than in Flash by 1–2 h. The particularity of Java is related to the increasing phase of the diurnal cycle of Prec (6 h), which is faster than over all the other land areas considered in our study (7 – 8 h). The

345 strong and rapid convective growing phase measured over Java might be explained by the fact that the island is narrow with high mountains (up to ~ 2000 m of altitude, as shown in Fig. 2b) reaching the coast. The topography promotes the growth of intense and rapid convective activity. The convection starts around 09:00 LT, rapidly elevating warm air up to the top of the mountains. Around 15:00 LT, air masses cooled in altitude are transported to the sea favoring the dissipating stage of the convection. Sulawesi is also a small island with high topography as Java. However, the amplitude of the diurnal cycle of Prec

350 and Flash is not as strong as over Java. Other islands, such as Borneo, New Guinea and Sumatra, have high mountains but also large lowland areas. Mountains promote deep convection at the beginning of the afternoon while lowlands help maintain the convective activity through shallow convection and stratiform rainfall (Nesbitt and Zipser, 2003; Qian, 2008). Deep and shallow convection are then mixed during the slow dissipating phase of the convection (from $\sim 16:00$ LT to 08:00 LT). However, because Flash are observed only in deep convective clouds, the decreasing phase of Flash diurnal cycles decreases

355 more rapidly than the decreasing phase of Prec. The diurnal maxima of Prec found separately over the 5 islands of the MariCont (at $0.25^\circ \times 0.25^\circ$ resolution) are much higher than the diurnal maxima of Prec found over tropical land (South America, South Africa and MariCont_L, at $2^\circ \times 2^\circ$ resolution) from Dion et al. (2019): $\sim 0.6 - 1.0 \text{ mm h}^{-1}$ and $\sim 0.4 \text{ mm h}^{-1}$, respectively. However, the duration of the increasing phase of the diurnal cycle of Prec is consistent with the one calculated over tropical land by Dion et al. (2019).

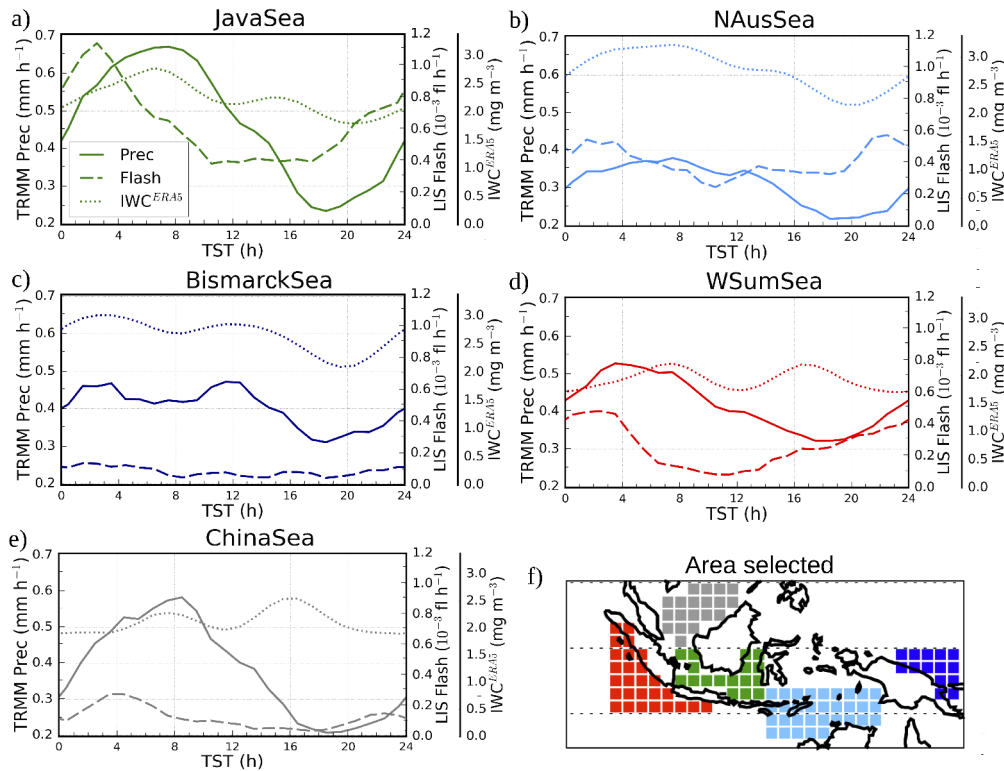


Figure 9. Diurnal cycles of Prec (solid line), Flash (dashed line) and IWC^{ERA5} from ERA5 at 150 hPa (dotted line) over MariCont seas: Java Sea (a), North Australia Sea (NAusSea) (b), Bismarck Sea (c), West Sumatra Sea (WSumSea) (d), China Sea (e) and map of the study zones over sea (f).

360 Over sea, the five selected areas (Fig. 9a–e) show a diurnal cycle of Prec and Flash similar to that of either coastline or offshore areas depending on the region considered. The diurnal cycle of Prec and Flash over Java Sea is similar to the one over coastlines (Fig. 7b). Java Sea (Fig. 9a), an area mainly surrounded by coasts, shows the largest diurnal maximum of Prec ($\sim 0.7 \text{ mm h}^{-1}$) and Flash ($\sim 1.1 \cdot 10^{-3} \text{ flashes h}^{-1}$) with the longest growing phase. In this area, land and sea breezes observed in coastal areas impact the diurnal cycle of the convection (Qian, 2008). During the night, land breeze develops from

365 a temperature gradient between warm sea surface temperature and cold land surface temperature and conversely during the day. Over Java Sea, Prec is strongly impacted by land breezes from Borneo and Java islands (Qian, 2008), explaining why Prec and Flash reach largest values during the early morning. By contrast, NAusSea, Sea and WSumSea (Figs. 9b, c and d, respectively) present small amplitude of diurnal cycle. In our analysis, these three study zones are the areas including the most offshore pixels. Java Sea and WSumSea present a similar diurnal cycle of Prec and Flash, with Flash growing phase starting
 370 about 4 h earlier than that of Prec. China Sea also shows a diurnal maximum of Flash shifted by about 4 hours before the diurnal maximum of Prec, but the time of the diurnal minimum of Prec and Flash is similar. Over China Sea and Bismarck Sea, the diurnal cycle of Flash shows a weak amplitude with maxima reaching only $0.1 - 0.2 \cdot 10^{-3}$ flashes h^{-1} . Furthermore, over the Sea, while the diurnal minimum in Prec is around 18:00 LT, there are several local minima in Flash (08:00, 14:00 and 18:00 LT). Over NAusSea, the diurnal minimum of Prec is delayed by more than 7 hours compared to the diurnal minimum of
 375 Flash.

To summarize, over islands, Flash and Prec convective increasing phases start at the same time and increase similarly but the diurnal maximum of Flash is reached 1–2 hours before the diurnal maximum of Prec. Over seas, the duration of the convective increasing phase and the amplitude of the diurnal cycles are not always similar depending on the area considered. The diurnal cycle of Flash over Java Sea and West Sumatra Sea is 4 hours ahead of the diurnal cycle of Prec, and over North Australia
 380 Sea, it is more than 7 hours ahead. China Sea and Bismarck Sea present the same time of the onset of the Flash and Prec increasing phase. In Section 7, we estimate ΔIWC over the 5 selected island and sea areas from Prec and Flash as a proxy of deep convection.

6 Horizontal distribution of IWC from ERA5 reanalyses

The ERA5 reanalysis provides hourly IWC at 150 and 100 hPa (IWC^{ERA5}). The diurnal cycle of IWC^{ERA5} over the MariCont
 385 will be used to calculate $\Delta\text{IWC}^{\text{ERA5}}$ in order to support the horizontal distribution and the amount of ice injected in the UT and the TL deduced from our model combining IWC^{MLS} and TRMM-3B42 Prec or IWC^{MLS} and LIS flash. Since IWC^{ERA5} data quality has not yet been fully evaluated, this may impact on the consistency or lack of thereof found in the comparisons between $\Delta\text{IWC}^{\text{ERA5}}$ and both $\Delta\text{IWC}^{\text{Prec}}$ and $\Delta\text{IWC}^{\text{Flash}}$. Figures 10a, b, c and d present the daily mean and the hour of the diurnal maxima of IWC^{ERA5} at 150 and 100 hPa. In the UT, the daily mean of IWC^{ERA5} shows a horizontal distribution over
 390 the MariCont consistent with that of IWC^{MLS} (Fig. 2e), except over New Guinea where IWC^{ERA5} (exceeding 6.4 mg m^{-3}) is much stronger than IWC^{MLS} ($\sim 4.0 \text{ mg m}^{-3}$). The highest amount of IWC^{ERA5} is located over New Guinea mountain chain and in the West coast of North Australia (exceeding 6.4 mg m^{-3} in the UT and 1.0 mg m^{-3} in the TL). Over islands in the UT and the TL, the hour of the IWC^{ERA5} diurnal maximum is found between 12:00 LT and 15:00 LT over Sulawesi and New Guinea and between 15:00 LT and 21:00 LT over Sumatra, Borneo and Java, which is close to the hour of the diurnal
 395 maximum of Flash over islands (Fig. 6). Over sea, in the UT and the TL, the hour of the IWC^{ERA5} diurnal maximum is found between 06:00 LT and 09:00 LT over West Sumatra Sea, Java Sea, North Australia Sea, between 06:00 LT and 12:00 LT over

China Sea and between 00:00 LT and 03:00 LT over Bismarck Sea. There are no significant differences between the hour of the maximum of IWC^{ERA5} in the UT and in the TL.

The diurnal cycles of IWC^{ERA5} at 150 hPa are presented in Figs. 8 and 9 over the selection of islands and seas of the MariCont together with the diurnal cycles of Prec and Flash. Over islands (Fig. 8), the maximum of the diurnal cycle of IWC^{ERA5} is found between 16:00 LT and 17:00 LT, consistent with the diurnal cycle of Prec and Flash. The durations of the increasing phase of the diurnal cycles of Prec, Flash and IWC^{ERA5} are all consistent to each other (6 – 8 h). Over sea (Fig. 9), the maximum of the diurnal cycle of IWC^{ERA5} is mainly found between 07:00 LT and 10:00 LT over Java Sea and North Australia Sea, consistent with the diurnal cycle of Prec, and a second peak is found around 16:00 LT. Thus, the duration of the increasing phase of the diurnal cycles of IWC^{ERA5} is consistent with the one of Prec over these two sea study zones (~10 hours), but not with the one of Flash. Over Bismarck Sea, the diurnal maxima of IWC^{ERA5} are found at 04:00 LT with a second peak later at noon. Over West Sumatra Sea, two diurnal maxima are found at 08:00 LT and 17:00 LT. Over China Sea, the diurnal maximum of IWC^{ERA5} is found at 16:00 LT with a second peak at 08:00 LT. These differences in the timing of the maximum of the diurnal cycle of Prec, Flash and IWC^{ERA5} observed at small-scale over sea of the MariCont are not well understood. However, these differences do not impact on the calculation of the ΔIWC^{Prec} , ΔIWC^{Flash} or ΔIWC^{ERA5} , because only the magnitude of the diurnal cycle (max-min) matters for the calculation of ΔIWC .

7 Ice injected over a selection of island and sea areas

Figure 11 synthesizes ΔIWC deduced from observations and reanalysis in the UT and the TL over the 5 islands and 5 seas of the MariCont studied in the previous section.

7.1 ΔIWC deduced from observations

Eqs. (1-3) are used to calculate ΔIWC from Prec (ΔIWC^{Prec}) and from Flash (ΔIWC^{Flash}). As presented in the previous section, Prec and Flash can be used as two proxies of deep convection, although differences in their diurnal cycles may be present as a function of the region considered. Thus, the observational ΔIWC range calculated between ΔIWC^{Prec} and ΔIWC^{Flash} provides an upper and lower bound of ΔIWC calculated from observational datasets. In the following, we will consider the relative difference between ΔIWC^{Prec} and ΔIWC^{Flash} as:

$$r^{Prec-Flash} = 100 \times \frac{\Delta IWC^{Prec} - \Delta IWC^{Flash}}{(\Delta IWC^{Prec} + \Delta IWC^{Flash}) \times 0.5} \quad (4)$$

In the UT (Fig. 11a), over islands, ΔIWC calculated over Sumatra, Borneo, Sulawesi and New Guinea varies from 4.9 to 6.9 mg m^{-3} whereas, over Java, ΔIWC reaches 7.9–8.7 mg m^{-3} . ΔIWC^{Flash} is generally greater than ΔIWC^{Prec} by 0.8 mg m^{-3} (with $r^{Prec-Flash}$ ranges from - 6 to - 22% over the study zone) for all the islands, except for Java where ΔIWC^{Prec} is larger than ΔIWC^{Flash} by 0.8 mg m^{-3} ($r^{Prec-Flash} = 7.1\%$). Over sea, ΔIWC varies from 1.2 to 4.4 mg m^{-3} . ΔIWC^{Flash} is greater than ΔIWC^{Prec} by 0.6 to 2.1 mg m^{-3} ($r^{Prec-Flash} = - 35$ to - 71%), except for Java Sea, where ΔIWC^{Prec} is

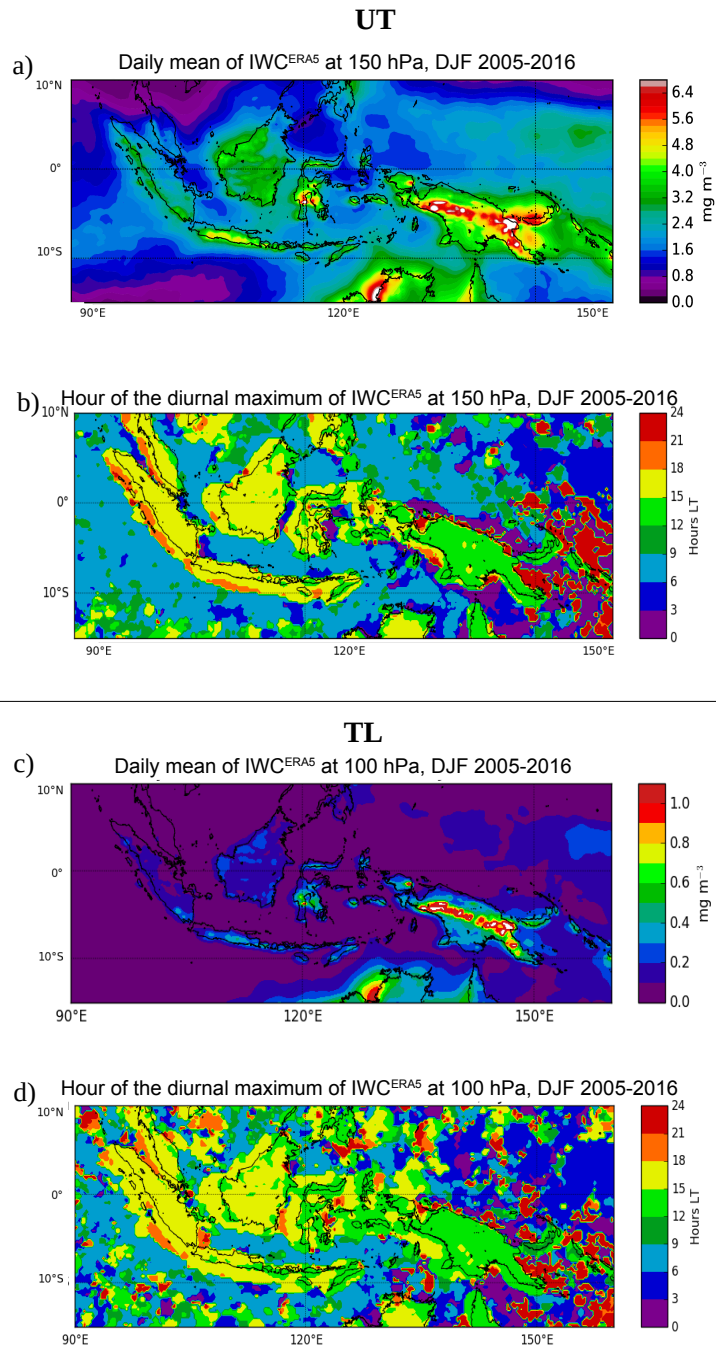


Figure 10. Daily mean of IWC^{ERA5} averaged over the period DJF 2005-2016 at 150 hPa (a) and at 100 hPa (c); Time (hour, local time (LT)) of the diurnal maximum of IWC^{ERA5} at 150 hPa (b) and at 100 hPa (d).

greater than ΔIWC^{Flash} by 0.2 mg m^{-3} ($r^{Prec-Flash} = 6\%$). Over North Australia Sea and West Sumatra Sea, ΔIWC^{Flash} are more than twice as large as ΔIWC^{Prec} ($r^{Prec-Flash} = -63\%$ and -71% , respectively).

In the TL (Fig. 11b), the observational ΔIWC range is found between 0.7 and 1.3 mg m^{-3} over islands and between 0.2 and 0.7 mg m^{-3} over seas. The same conclusions apply to the observational ΔIWC range calculated between ΔIWC^{Prec} and ΔIWC^{Flash} in the TL as in the UT with differences less than 0.4 mg m^{-3} .

To summarize, independently of the proxies used for the calculation of ΔIWC , and at both altitudes, Java island shows the largest injection of ice over the MariCont. Observational ΔIWC over Java island is larger by about 1.0 mg m^{-3} in the UT and about 0.3 mg m^{-3} in the TL than other land study zones. Furthermore, it has been shown that both proxies can be used in our model, with more confidence over land: ΔIWC^{Prec} and ΔIWC^{Flash} are consistent to each other to within $r^{Prec-Flash} = -6$ to -22% over islands and $r^{Prec-Flash} = +6$ to -71% over seas in the UT and the TL. The largest difference over seas is probably due to the larger contamination by stratiform precipitation included in Prec over sea.

7.2 ΔIWC deduced from reanalysis

ΔIWC from ERA5 ($\Delta IWC_{z_0}^{ERA5}$) is calculated in the UT and the TL ($z_0 = 150$ and 100 hPa, respectively) as the max–min difference in the amplitude of the diurnal cycle. We can use the IWC^{ERA5} to assess the impact of the vertical resolution of the MLS measurements on the observationally-derived ΔIWC estimates. According to Wu et al. (2008), estimates of IWC derived from MLS represent spatially-averaged quantities within a volume that can be approximated by a box of $\sim 300 \times 7 \times 4 \text{ km}^3$ near the pointing tangent height. In order to compare IWC^{MLS} and IWC^{ERA5} , two steps were taken: 1) the horizontal resolution of ERA5 was degraded from $0.25^\circ \times 0.25^\circ$ to $2^\circ \times 2^\circ$ ($\sim 200 \text{ km} \times 200 \text{ km}$), and 2) the vertical resolution of ERA5 was degraded by convolving the vertical profiles of IWC^{ERA5} with a box function whose width is 5 and 4 km at 100 and 146 hPa, respectively. The ice injected from ERA5 at $z_0 = 146$ and 100 hPa with degraded vertical resolution ($\langle \Delta IWC_{z_0}^{ERA5} \rangle$) is thus calculated from $\langle IWC_{z_0}^{ERA5} \rangle$. In the following we can consider the difference $r^{ERA5-\langle ERA5 \rangle}$ between ΔIWC^{ERA5} and $\langle \Delta IWC^{ERA5} \rangle$ as:

$$r^{ERA5-\langle ERA5 \rangle} = 100 \times \frac{\Delta IWC^{ERA5} - \langle \Delta IWC^{ERA5} \rangle}{(\Delta IWC^{ERA5} + \langle \Delta IWC^{ERA5} \rangle) \times 0.5} \quad (5)$$

Figure 11 shows $\Delta IWC_{z_0}^{ERA5}$ and $\langle \Delta IWC_{z_0}^{ERA5} \rangle$ at $z_0 = 150$ and 100 hPa, over the island and the sea study zones. In the UT (Fig. 11a), over islands, ΔIWC_{150}^{ERA5} and $\langle \Delta IWC_{150}^{ERA5} \rangle$ calculated over Sumatra and Borneo vary from 4.9 to 7.0 mg m^{-3} ($r^{ERA5-\langle ERA5 \rangle}$ ranges from 20 to 22%) whilst ΔIWC_{150}^{ERA5} and $\langle \Delta IWC_{150}^{ERA5} \rangle$ over Java, Sulawesi and New Guinea reach 7.5 – 10.0 mg m^{-3} ($r^{ERA5-\langle ERA5 \rangle} = 21$ to 24%). Over sea, ΔIWC_{150}^{ERA5} and $\langle \Delta IWC_{150}^{ERA5} \rangle$ vary from 0.35 to 1.1 mg m^{-3} ($r^{ERA5-\langle ERA5 \rangle} = 9$ to 33%). Over island and sea, ΔIWC_{150}^{ERA5} is greater than $\langle \Delta IWC_{150}^{ERA5} \rangle$. The small differences between ΔIWC_{150}^{ERA5} and $\langle \Delta IWC_{150}^{ERA5} \rangle$ over island and sea in the UT support the fact that the vertical resolution at 150 hPa has a low impact on the estimated ΔIWC .

In the TL, over land, ΔIWC_{100}^{ERA5} and $\langle \Delta IWC_{100}^{ERA5} \rangle$ vary from 0.5 to 3.9 mg m^{-3} ($r^{ERA5-\langle ERA5 \rangle} = -32$ to -138%) with $\langle \Delta IWC_{100}^{ERA5} \rangle$ being larger than ΔIWC_{100}^{ERA5} by less than 2.5 mg m^{-3} . Over sea, ΔIWC_{100}^{ERA5} and $\langle \Delta IWC_{100}^{ERA5} \rangle$ vary

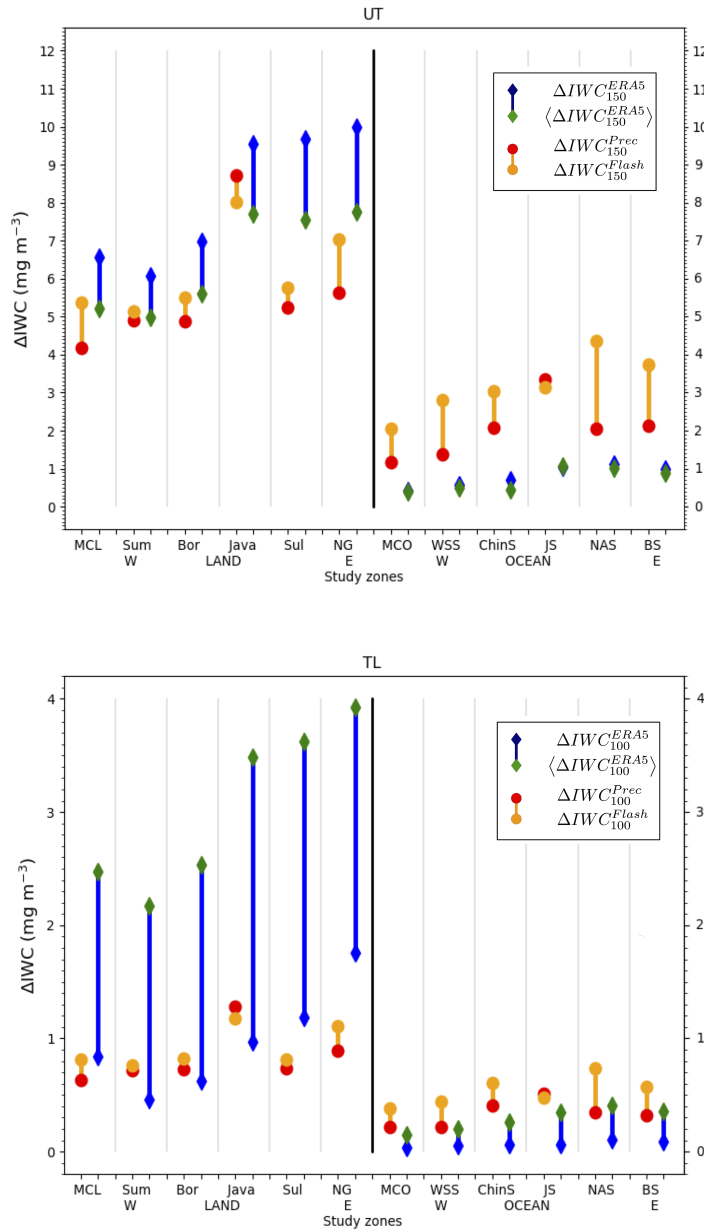


Figure 11. Top: ΔIWC (mg m^{-3}) estimated from Prec (red) and Flash (orange) at 146 hPa and ΔIWC estimated from ERA5 at the level 150 hPa and at the level 150 hPa degraded in the vertical, over islands and seas of the MariCont: MariCont_L (MCL) and MariCont_O (MCO); from West (W) to East (E) over land, Sumatra (Sum), Borneo (Bor), Java, Sulawesi (Sul) and New Guinea (NG); and over seas, West Sumatra Sea (WSS), China Sea (ChinS), Java Sea (JS), North Australia Sea (NAS) and Sea (BS). Bottom: Same as in top but for 100 hPa.

from 0.05 to 0.4 mg m⁻³ ($r^{ERA5-\langle ERA5 \rangle} = -85$ to -139%) with ΔIWC_{100}^{ERA5} lower than $\langle \Delta IWC_{100}^{ERA5} \rangle$ by as much as 0.2
460 mg m⁻³. The large differences between ΔIWC_{100}^{ERA5} and $\langle \Delta IWC_{100}^{ERA5} \rangle$ over island and sea in the TL support the fact that
the vertical resolution at 100 hPa has a high impact on the estimation of ΔIWC .

7.3 Synthesis

The comparison between the observational ΔIWC range and the reanalysis ΔIWC range is presented in Fig. 11. In the UT,
over land, observation and reanalysis ΔIWC ranges agree to within 0.1 to 1.0 mg m⁻³, which highlights the robustness of our
465 model over land, except over Sulawesi and New Guinea, where the observational and the reanalysis ΔIWC range differ by at
least 1.7 and 0.7 mg m⁻³, respectively. Over sea, the observational ΔIWC range is systematically greater than the reanalysis
by $\sim 1.0 - 2.2$ mg m⁻³, showing a systematic larger estimate derived from observation than derived from reanalysis. The
consistency between observational and reanalysis ΔIWC range is calculated as the difference between the minimal value of
the largest range minus the maximum value of the lowest range divided by the mean of these two values. In the UT, over land,
470 observational and reanalysis ΔIWC are found consistent to within 0 to 25% while over sea they are inconsistent (to within 62
to 96%) in the UT. In the TL, observational and reanalysis ΔIWC ranges are consistent to within 0 to 49% over land and to
within 0 to 28% over sea. In the following we will consider r^{Total} as the relative differences between the minimal value of
the lower range minus the maximum value of the largest range divided by the mean of these two values. The range between
observational and reanalysis ranges is named the total IWC range, and is estimated in the UT between 4.2 and 10.0 mg m⁻³
475 (r^{Total} from 8 to 59%) over land and between 0.3 and 4.4 mg m⁻³ (r^{Total} from 104 to 149%) over sea and, in the TL, between
0.5 and 3.7 mg m⁻³ ($r^{Total} = 85$ to 127%) over land, and between 0.1 and 0.7 mg m⁻³ ($r^{Total} = 142$ to 160%) over sea.

Amounts of ice injected deduced from observations and reanalysis are consistent to each other over land in the UT and over
land and sea in the TL (to within 0 to 49%) but inconsistent over sea in the UT (up to 96%). However, the impact of the vertical
resolution on the estimation of ΔIWC is much larger in the UT than in the TL (r^{Total} is larger in the TL than in the UT). At
480 both levels, observational and reanalyses ΔIWC estimated over land is more than twice as large as ΔIWC estimated over sea.
Java island presents the highest observational and reanalysis ΔIWC range in the UT (between 7.7 and 9.5 mg m⁻³ daily mean,
 $r^{Total} = 21\%$). However, whatever the level considered, although Java has shown particularly high values in the observational
 ΔIWC range compared to other study zones, the reanalysis ΔIWC range shows that Sulawesi and New Guinea would also be
able to reach similar high values of ΔIWC as Java (assuming that ERA5 IWC data have not yet been evaluated).

485 8 Discussion on small-scale convective processes impacting ΔIWC over a selection of areas

Our results have shown that, in all the datasets used, Java island and Java Sea are the two areas with the largest amount of ice
injected up to the UT and the TL over the MariCont land and sea, respectively. In this section, processes impacting ΔIWC in
the different study zones are discussed.

8.1 Java island, Sulawesi and New Guinea

490 Sulawesi, New Guinea and particularly Java island have been shown as the areas of the largest ΔIWC in the UT and TL. Qian (2008) have used high resolution observations and regional climate model simulations to show the three main processes impacting the diurnal cycle of rainfall over the Java island. The main process explaining the rapid and strong peak of Prec during the afternoon over Java (Fig. 8a) is the sea-breeze convergence around midnight. This convergence caused by sea-breeze phenomenon increases the deep convective activity and impacts on the diurnal cycle of Prec and on the IWC injected up to the
495 TL by amplifying their quantities. The second process is the mountain-valley wind converging toward the mountain peaks, and reinforcing the convergence and the precipitation. The land breeze becomes minor compared to the mountain-valley breeze and this process is amplified with the mountain altitude. As shown in Fig. 2b, New Guinea has the highest mountain chain of the MariCont. The third process shown by Qian (2008) is precipitation that is amplified by the cumulus merging processes which are processes more important over small islands such as Java (or Sulawesi) than over large islands such as Borneo
500 or Sumatra. Another process is the interaction between sea-breeze and precipitation-driven cold pools that generates lines of strong horizontal moisture convergence (Dauhut et al., 2016). Thus, IWC is increasing proportionally with Prec consistent with the results from Dion et al. (2019) and rapid convergence combined with deep convection transports elevated amounts of IWC at 13:30 LT (Fig. 3) producing high ΔIWC during the growing phase of the convection (Fig. 4 and Fig. 11) over Java Island.

8.2 West Sumatra Sea

505 In section 4.2, it has been shown that the West Sumatra Sea is an area with positive anomaly of Prec during the growing phase of the convection but negative anomaly of IWC, which differs from other places. These results suggest that Prec is representative not only of convective precipitation but also of stratiform precipitation. The diurnal cycle of stratiform and convective precipitations over West Sumatra Sea has been studied by Mori et al. (2004) using 3 years of TRMM precipitation radar (PR) datasets, following the 2A23 Algorithm (Awaka, 1998). Mori et al. (2004) have shown that rainfall over Sumatra is
510 characterized by convective activity with a diurnal maximum between 15:00 LT and 22:00 LT while, over the West Sumatra Sea, the rainfall type is convective and stratiform, with a diurnal maximum during the early morning (as observed in Fig. 9). Furthermore, their analyses have shown a strong diurnal cycle of 200-hPa wind, humidity and stability, consistent with the PR over West Sumatra Sea and Sumatra Island. Stratiform and convective clouds are both at the origin of heavy rainfall in the tropics (Houze and Betts, 1981; Nesbitt and Zipser, 2003) and in the West Sumatra Sea, but stratiform clouds are mid-altitude
515 clouds in the troposphere and do not transport ice up to the tropopause. Thus, over the West Sumatra Sea, the calculation of ΔIWC estimated from Prec is possibly overestimated because Prec include a non-negligible amount of stratiform precipitation over this area.

8.3 North Australia Sea and seas with nearby islands

The comparisons between Figs. 2c and 6a have shown strong daily mean of Flash (10^{-2} – 10^{-1} flashes day⁻¹) but low daily
520 mean of Prec (2.0 – 8.0 mm day⁻¹) over the North Australia Sea. Additionally, Fig. 11 shows that the strongest differences

between ΔIWC^{Prec} and ΔIWC^{Flash} are found over the North Australia Sea, with ΔIWC^{Flash} greater than ΔIWC^{Prec} by 2.3 mg m^{-3} in the UT ($r^{Prec-Flash} = \sim 71\%$) and by 0.4 mg m^{-3} in the TL ($r^{Prec-Flash} = -75\%$). These results imply that the variability range in our model is too large highlighting the difficulty to estimate ΔIWC over this study zone. Furthermore, as for Java Sea or Bismarck Sea, North Australia Sea is surrounded by several islands. According to the study from Pope et al. (2008), the cloud size is the largest during the afternoon over the North Australia land, during the night over North Australia coastline and during the early morning over the North Australia sea. These results suggest that deep convective activity moves from the land to the sea during the night. Over the North Australia Sea, it seems that the deep convective clouds are mainly composed of storms with lightning but precipitation is weak or does not reach the surface before evaporating.

9 Conclusions

The present study has combined observations of ice water content (IWC) measured by the Microwave Limb Sounder (MLS), precipitation (Prec) from the algorithm 3B42 of the Tropical Rainfall Measurement Mission (TRMM), the number of flashes (Flash) from the Lightning Imaging Sensor (LIS) on board of TRMM with IWC provided by the ERA5 reanalyses in order to estimate the amount of ice injected (ΔIWC) in the upper troposphere (UT) and the tropopause level (TL) over the MariCont, from the method proposed in a companion paper (Dion et al., 2019). The study is focused on the austral convective season of DJF from 2004 to 2017. In the model used (Dion et al., 2019), Prec is considered as a proxy of deep convection injecting ice (ΔIWC^{Prec}) in the UT and the TL. ΔIWC^{Prec} is firstly calculated by the correlation between the growing phase of the diurnal cycle of Prec from TRMM-3B42 (binned at a 1-hour diurnal cycle) and the value of IWC measured by MLS (IWC^{MLS} , provided at the temporal resolution of 2 observations in local time per day) selected among the growing phase of the diurnal cycle of Prec. While Dion et al. (2019) have calculated ΔIWC^{Prec} over large convective study zones in the tropics, we show the spatial distribution of ΔIWC^{Prec} in the UT and the TL at $2^\circ \times 2^\circ$ horizontal resolution over the MariCont, highlighting local areas of strong injection of ice up to 20 mg m^{-3} in the UT and up to 3 mg m^{-3} in the TL. ΔIWC injected in the UT and the TL has also been evaluated by using another proxy of deep convection: Flash measured by TRMM-LIS. Diurnal cycle of Flash has been compared to diurnal cycle of Prec, showing consistencies in 1) the spatial distribution of Flash and Prec over the MariCont (maxima of Prec and Flash located over land and coastline), and 2) their diurnal cycles over land (similar onset and duration of the diurnal cycle increasing phase). Differences have been mainly observed over sea and coastline areas, with the onset of the diurnal cycle increasing phase of Prec delayed by several hours depending on the considered area (from 2 to 7 h) compared to Flash. ΔIWC calculated by using Flash as a proxy of deep convection (ΔIWC^{Flash}) is compared to ΔIWC^{Prec} over five islands and five seas of the MariCont to establish an observational ΔIWC range over each study zone. ΔIWC is also estimated from IWC provided by the ERA5 reanalyses (ΔIWC^{ERA5} and IWC^{ERA5} , respectively) at 150 and 100 hPa over the study zones. We have also degraded the vertical resolution of IWC^{ERA5} to be consistent with that of IWC^{MLS} observations: 4 km at 146 hPa and 5 km at 100 hPa. The ΔIWC ranges calculated from observations and reanalyses were evaluated over the selected study zones (island and sea).

With the study of ΔIWC^{Prec} , results show that the largest amounts of ice injected in the UT and TL per $2^\circ \times 2^\circ$ pixels are related to i) an amplitude of Prec diurnal cycle larger than 0.5 mm h^{-1} and ii) a duration of the growing phase of the convection longer than 9 hours. The largest ΔIWC^{Prec} has been found over areas where the convective activity is the deepest. ΔIWC^{Prec} and ΔIWC^{Flash} depart from -6 to -22 % over land and to -6 to -71 % over sea. The largest differences between ΔIWC^{Prec} and ΔIWC^{Flash} over sea might be due to the combination of the presence of stratiform precipitation included in Prec and the very low values of Flash over seas ($<10^{-2}$ flashes day^{-1}). The diurnal cycle of IWC^{ERA5} at 150 hPa is more consistent with that of Prec and Flash over land than over ocean. Finally, ΔIWC estimated from observations has been shown to be consistent with ΔIWC estimated from reanalysis to within 25% over land in the UT, to within 49 % over land in the TL and to within 28 % over sea in the TL, but inconsistent to within 96 % over sea in the UT. Thus, thanks to the combination of the observational and reanalysis ΔIWC ranges, the total ΔIWC range has been found in the UT to be between 4.2 and 10.0 mg m^{-3} over land and between 0.3 and 4.4 mg m^{-3} over sea and, in the TL, between 0.5 and 3.7 mg m^{-3} over land and between 0.1 and 0.7 mg m^{-3} over sea. The impact of the vertical resolution on the estimation of ΔIWC has been found higher in the TL than in the UT.

The study at small scale over islands and seas of the MariCont has shown that ΔIWC from ERA5, Prec and Flash in the UT agree to within $0.1 - 1.0 \text{ mg m}^{-3}$ over MariCont_L, Sumatra, Borneo and Java with the largest values obtained over Java Island. Based on observations, the Java Island presents the largest amount of ice in the UT and the TL (larger by about 1.0 mg m^{-3} in the UT and about 0.3 mg m^{-3} in the TL than other land study zones). Based on the reanalysis, New Guinea and Sulawesi reach similar ranges of ice injection in the UT and even larger ranges of values in the TL than the Java Island keeping in mind that ERA5 IWC data have not yet been evaluated. Processes related to the strongest amount of ΔIWC injected into the UT and the TL have been identified as the combination of sea-breeze, mountain-valley breeze and merged cumulus, accentuated over small islands with high topography such as Java or Sulawesi.

Author contributions. IAD analysed the data, formulated the model and the method combining MLS, TRMM and LIS data and took primary responsibility for writing the paper. CD has treated the LIS data, provided the Figures with Flash datasets, gave advices on data processing and contributed to the Prec and Flash comparative analysis. PR strongly contributed to the design of the study, the interpretation of the results and the writing of the paper. PR, FC, PH and TD provided comments on the paper and contributed to its writing.

Acknowledgements. We thank the National Center for Scientific Research (CNRS) and the Excellence Initiative (Idex) of Toulouse, France to fund this study and the project called Turbulence Effects on Active Species in Atmosphere (TEASAO – <http://www.legos.obs-mip.fr/projets/axes-transverses-processus/teasao>, last access: May 2020, Peter Haynes Chair of Attractivity). We would like to thank the teams that have provided the MLS data (https://disc.gsfc.nasa.gov/datasets?page=1&keywords=ML2IWC_004, last access: May 2020), the TRMM data (<https://pmm.nasa.gov/data-access/downloads/trmm>), the LIS data (https://ghrc.nsstc.nasa.gov/lightning/data/data_lis_trmm.html, last access: May 2020) and the ERA5 Reanalysis data (<https://cds.climate.copernicus.eu/cdsapp#!/dataset/reanalysis-era5-pressure-levels-monthly-means?>

tab=form, last access: May 2020). We would like to thank both reviewers for their helpful comments and especially Michelle Santee for the
585 many very detailed comments she provided that were invaluable in improving the study.

Main acronyms list

ΔIWC : Amount of ice injected by deep convection up to the study pressure level

ΔIWC^{Prec} : ΔIWC estimated from Prec and from IWC^{MLS}

ΔIWC^{Flash} : ΔIWC estimated from Flash and from IWC^{MLS}

590 ΔIWC^{ERA5} : ΔIWC estimated from ERA5 reanalysis

$\langle \Delta IWC^{ERA5} \rangle$: ΔIWC^{ERA5} degraded along the vertical at the study pressure level consistently with the MLS vertical resolution of IWC^{MLS}

DJF: December, January, February

Flash: number of Flashes

595 IWC: Ice water content

IWC^{ERA5} : IWC from ERA5 reanalysis

IWC^{MLS} : IWC measured by MLS

LS: Lower stratosphere

MariCont: Maritime Continent

600 MariCont_C: Coastlines of the Maritime Continent

MariCont_O: Maritime Continent ocean

MariCont_L: Maritime Continent land

MLS: Microwave Limb Sounder

NAuSea: North Australia Sea

605 Prec: Precipitation

TTL: Tropical tropopause Layer

UT: Upper troposphere

UTLS: Upper troposphere and lower stratosphere

WSumSea: West Sumatra Sea

610 WV: Water vapour

References

- Awaka, J.: Algorithm 2A23 - Rain type classification. Proc. Symp. on the Precipitation Observation from Non-Sun Synchronous Orbit, 215–220, 1998.
- 615 Carbone, R. E., Wilson, J. W., Keenan, T. D. and Hacker, J. M.: Tropical island convection in the absence of significant topography, part I: life cycle of diurnally forced convection. *Monthly weather review*, 128(10):3459–3480, 2000.
- Chappel, L.: Assessing severe thunderstorm potential days and storm types in the tropics. Presentation at the International Workshop on the Dynamics and Forecasting of Tropical Weather Systems, Darwin, 2001.
- Christian, H. J. , Blakeslee, R. J., Goodman, S. J.: Lightning Imaging Sensor (LIS) for the international space station. In American Institute
620 of Physics Conference Proceedings, Vol. 504, No. 1, pp. 423-428, 2000.
- Dauhut, T. ,Chaboureau, J.-P. , Escobar, J. and Mascart, P.: Giga-LES of Hector the Convecteur and its two tallest updrafts up to the stratosphere. *Journal of the Atmospheric Sciences*, 73(12):5041–5060, 2016.
- Dauhut, T. , Chaboureau, J.-P., Mascart, P. and Lane, T.: The overshoots that hydrate the stratosphere in the tropics. EGU General Assembly Conference Abstracts, volume 20, 9149, 2018.
- 625 Dion, I.-A., Ricaud, P. , Haynes, P. , Carminati, F. and Dauhut, T.: Ice injected into the tropopause by deep convection – part 1: in the austral convective tropics. *Atmospheric Chemistry and Physics*, 19(9):6459–6479, 2019.
- Duncan, D., Eriksson, P.: An update on global atmospheric ice estimates from observations and reanalyses. In EGU General Assembly Conference Abstracts (Vol. 20, p. 13448), 2018.
- Fueglistaler, S., Dessler, A. E., Dunkerton, T. J., Folkins, I., Fu, Q. and Mote, P. W.: Tropical tropopause layer. *Reviews of Geophysics*, 47(1),
630 doi: 10.1029/2008RG000267, 2009a.
- Geer, A. J., Baordo, F., Bormann, N., Chambon, P., English, S. J. , Kazumori, M. et al.: The growing impact of satellite observations sensitive to humidity, cloud and precipitation. *Quarterly Journal of the Royal Meteorological Society*, 143(709), 3189-3206, 2017.
- Goler, R., Reeder, M. J., Smith, R. K., Richter, H., Arnup, S., Keenan, T., May, P. and Hacker, J.: Low-level convergence lines over North Eastern Australia. part I: the North Australian cloud line. *Monthly weather review*, 134(11):3092–3108, 2006.
- 635 Hatsushika, H. and Yamazaki, K.: Inter-annual variations of temperature and vertical motion at the tropical tropopause associated with ENSO. *Geophysical research letters*, 28(15):2891–2894, 2001.
- Hersbach, H.:Operational global reanalysis: progress, future directions and synergies with NWP. European Centre for Medium Range Weather Forecasts, 2018.
- Houze, R. A. and Betts, A. K.: Convection in gate. *Reviews of Geophysics*, 19(4):541–576, 1981.
- 640 Huffman, G. J. ,Bolvin, D. T., Nelkin, E. J., Wolff, D. B., Adler, R. F., Gu, G., Hong, Y., Bowman, K. P. and Stocker, E. F.: The TRMM multi-satellite precipitation analysis (TMPA): quasi-global, multiyear, combined-sensor precipitation estimates at fine scales. *Journal of hydrometeorology*, 8(1):38–55, 2007.
- Huffman, G. J., Adler, R. F., Bolvin, D. T., Nelkin, E. J.: The TRMM Multi-satellite Precipitation Analysis (TMPA) in Satellite rainfall applications for surface hydrology. Springer, Dordrecht, 3-22, 2010.
- 645 Huffman, G. J., Bolvin, D. T.: Real-time TRMM Multi-satellite Precipitation Analysis data set documentation. Available online: URL https://gpm.nasa.gov/sites/default/files/document_files/3B4XRT_doc_V7_180426.pdf (last access: April 2020).
- Jensen, E. J., Ackerman, A. S., Smith, J. A.: Can overshooting convection dehydrate the tropical tropopause layer?. *Journal of Geophysical Research: Atmospheres*, 112(D11), 2007.

- Liu, C. and Zipser, E. J.: Global distribution of convection penetrating the tropical tropopause. *Journal of Geophysical Research: Atmospheres*, 110(D23), 2005.
- Liu, C. and Zipser, E. J.: Diurnal cycles of precipitation, clouds, and lightning in the tropics from 9 years of TRMM observations. *Geophys. Res. Lett.*, 35, L04819, doi:10.1029/2007GL032437, 2008.
- Livesey, N. J., Read, W. G., Wagner, P. A., Froidevaux, L., Lambert, A., Manney, G.L., Millan, L.F., Pumphrey, H. C., Santee, M. L., Schwartz, M. J., Wang, S., Fuller, R. A., Jarnot, R. F., Knosp, B. W., Martinez, E. and Lay, R. R.: Version 4.2x Level 2 data quality and description document, Tech. Rep. JPL D-33509 Rev. D, Jet Propulsion Laboratory, available at:<http://mls.jpl.nasa.gov> (last access: 01 09 2019), 2018.
- Lopez, P.: Direct 4D-Var assimilation of NCEP stage IV radar and gauge precipitation data at ECMWF. *Monthly Weather Review*, 139(7), 2098-2116, 2011.
- Love, B. S., Matthews, A. J. and Lister, G. M. S.: The diurnal cycle of precipitation over the Maritime Continent in a high-resolution atmospheric model. *Quarterly Journal of the Royal Meteorological Society*, 137(657):934–947, 2011.
- Millán, L., Read, W., Kasai, Y., Lambert, A., Livesey, N., Mendrok, J., Sagawa, H., Sano, T., Shiotani, M. and Wu, D. L.: SMILES ice cloud products. *Journal of Geophysical Research: Atmospheres*, 118(12):6468–6477, 2013.
- Mori, S., Jun-Ichi, H., Tauhid, Y. I., Yamanaka, M. D., Okamoto, N., Murata, F., Sakurai, N., Hashiguchi, H. and Sribimawati, T.: Diurnal land–sea rainfall peak migration over Sumatra island, Indonesian Maritime Continent, observed by TRMM satellite and intensive radio sonde soundings. *Monthly Weather Review*, 132(8):2021–2039, 2004.
- Nesbitt S. W. and Zipser, E. J.: The diurnal cycle of rainfall and convective intensity according to three years of TRMM measurements. *Journal of Climate*, 16(10):1456–1475, 2003.
- Petersen, W. A. and Rutledge, S. A.: Regional variability in tropical convection: observations from TRMM. *Journal of Climate*, 14(17), 3566-3586, 2001.
- Pope, M, Jakob, C. and Reeder, M. J.: Convective systems of the North Australian monsoon. *Journal of Climate*, 21(19):5091–5112, 2008.
- Qian, J.-H.: Why precipitation is mostly concentrated over islands in the Maritime Continent. *Journal of the Atmospheric Sciences*, 65(4):1428–1441, 2008.
- Ramage, C. S.: Role of a tropical “Maritime Continent” in the atmospheric circulation. *Mon. Wea. Rev.*, 96(6):365–370, 1968.
- Randel, W. J., Wu, F., Voemel, H., Nedoluha, G. E. and Forster, P.: Decreases in stratospheric water vapor after 2001: links to changes in the tropical tropopause and the Brewer-Dobson circulation. *Journal of Geophysical Research: Atmospheres*, 111(D12), 2006a.
- Randel, W. J. and Jensen, E.J.: Physical processes in the tropical tropopause layer and their roles in a changing climate. *Nature Geoscience*, 6:169, 2013. doi: 10.1038/ngeo1733. URL <https://doi.org/10.1038/ngeo1733>, 2013.
- Sherwood, S. C.: A stratospheric “drain” over the Maritime Continent. *Geophysical research letters*, 27(5):677–680, 2000.
- Stenke A. and Grewe, V.: Simulation of stratospheric water vapor trends: impact on stratospheric ozone chemistry. *Atmospheric Chemistry and Physics*, 5(5): 1257–1272, 2005.
- Stephens G. L. and Greenwald, T. J.: The earth’s radiation budget and its relation to atmospheric hydrology: 2. observations of cloud effects. *Journal of Geophysical Research: Atmospheres*, 96(D8):15325–15340, 1991.
- Waters, J. W., Froidevaux, L., Harwood, R. S., Jarnot, R. F., Pickett, H. M., Read, W. G. ... and Holden, J. R.: The Earth Observing System Microwave Limb Sounder (EOS MLS) on the Aura satellite. *IEEE Transactions on Geoscience and Remote Sensing*, 44(5), 1075-1092, 2006.

Wu, D. L., Jiang, J. H., Read, W. G., Austin, R. T., Davis, C. P., Lambert, A., Stephens, G. L. and Vane, D. G., Waters, J. W.: Validation of the Aura MLS cloud ice water content measurements. *Journal of Geophysical Research: Atmospheres*, 113, D15, 2008.

Wu, D. L., Austin, R. T., Deng, M. et al. Comparisons of global cloud ice from MLS, CloudSat, and correlative data sets. *Journal of Geophysical Research: Atmospheres*, 2009, vol. 114, no D8, 2009.

690 Yang G.-Y. and Slingo, J.: The diurnal cycle in the tropics. *Monthly Weather Review*, 129(4):784–801, doi: 10.1175/1520-0493(2001), 2001.